The $\delta^{13}C$, $\delta^{18}O$ and Δ_{47} records in biogenic, pedogenic and geogenic carbonate types from paleosol-loess sequence and their paleoenvironmental meaning

Kazem Zamanian[1]* , Alex R. Lechler[2], Andrew J. Schauer[3], Yakov Kuzyakov[1,4,5], Katharine W. Huntington[3]*

[1]Department of Soil Science of Temperate Ecosystems, Department of Agricultural Soil Science, University of Göttingen, Büsgenweg 2, 37077 Göttingen, Germany
[2]Department of Geosciences, Pacific Lutheran University, Tacoma, WA, United States
[3]Department of Earth and Space Sciences and Quaternary Research Center, University of Washington, Seattle, WA, United States
[4]Institute of Environmental Sciences, Kazan Federal University, Kazan, Russia
[5]Agro-Technological Institute, RUDN University, 117198 Moscow, Russia
*Corresponding authors email addresses: zamanians@yahoo.com (K. Zamanian); kate1@uw.edu (K. W. Huntington)

Abstract

Paleoenvironmental reconstructions are commonly based on isotopic signatures of a variety of carbonate types, including rhizoliths and land-snail shells, present in paleosol-loess sequences. However, various carbonate types are formed through distinct biotic and abiotic processes over various periods, and therefore may record diverging environmental information in the same sedimentological layer. Here, we investigate the effects of carbonate type on $\delta^{13}C$, $\delta^{18}O$, and clumped isotope-derived paleotemperature [T(Δ_{47})] from the Quaternary Nussloch paleosol-loess sequence (Rhine Valley, SW Germany). $\delta^{13}C$, $\delta^{18}O$, and T(Δ_{47}) values of co-occurring rhizoliths (-8.2‰ to -5.8‰, -6.1‰ to -5.9‰, 12–32°C, respectively), loess dolls (-7.0‰, -5.6‰, 23°C), land-snail shells (-8.1‰ to -3.2‰, -4.0‰ to -2.2‰, 12–38°C), earthworm biospheroliths (-11‰, -4.7‰, 8°C), and "bulk" carbonates (-1.9‰ to -0.5‰, -5.6‰ to -5.3‰, 78–120°C) from three sediment layers depend systematically on the carbonate type, admixture from geogenic carbonate, and the duration of formation periods. Based on these findings, we provide a comprehensive summary for the application of the three isotopic proxies of $\delta^{13}C$, $\delta^{18}O$, and Δ_{47} in biogenic and pedogenic carbonates present in the same sediment layer to reconstruct paleoenvironments (e.g., local vegetation, evaporative conditions, and temperature). We conclude that bulk carbonates in Nussloch loess should be excluded from paleoenvironmental reconstructions. Instead, pedogenic and biogenic carbonates should be used to provide context for interpreting the isotopic signature for detailed site- and time-specific paleoenvironmental information.

Key words: Rhizoliths; Land-snail shells; Paleosol-loess sequence; Paleosol; Loess; Pedogenic carbonates; Clumped isotopes; Paleoenvironment reconstruction; CaCO3 formation

INTRODUCTION

Paleosol-loess sequences have a long history of use in paleoenvironmental reconstructions for a broad range of paleoclimate, geology, biology, and anthropology investigations (e.g., Riecken, 1950; Fisk, 1951; Kyuma et al., 1985; Wu et al., 2007; Zech et al., 2012; Lechler et al., 2018). The worldwide spatial distribution (Haase et al., 2007; Muhs, 2007; Roberts et al., 2013; Ghafarpour et al., 2016) and high temporal resolution (Frechen et al., 2003; Karimi et al., 2011; Sun et al., 2012; Taheri et al., 2016; Moine et al., 2017) of paleosol-loess sequences make them an important terrestrial archive (Guo et al., 2002). To this end, investigating isotopic compositions of carbon ($\delta^{13}C_{carb}$) and oxygen ($\delta^{18}O_{carb}$) of loess materials, and in particular carbonates formed in these sequences, has been a staple of paleoenvironmental reconstructions for decades. Carbonate $\delta^{13}C$ values provide information about paleovegetation (Quade and Cerling, 1995; Liu et al., 1996; Bayat et al., 2016), and $\delta^{18}O$ values are related to the temperature and the isotopic composition of oxygen in the soil water ($\delta^{18}O_{water}$) from which the carbonates precipitated (Cerling, 1984; Bayat et al., 2016; Lechler et al., 2018).

More recently, carbonate clumped isotope (Δ_{47}) thermometry has been used in terrestrial paleoclimate reconstructions (e.g., Affek, 2012; Eiler et al., 2014). Δ_{47} thermometry is an indicator of carbonate formation temperature independent of $\delta^{18}O_{water}$ through measure of the abundance of "clumped" carbonate molecules containing both ^{13}C and ^{18}O in excess of the abundance that would be expected if heavy isotopes were distributed randomly (Ghosh et al., 2006; Eiler, 2007). Recent applications of clumped isotope thermometry to study carbonates formed in or associated with paleosols and loess show the potential for using independent (paleo)temperature constraints to extract paleoclimate information from these records (Eagle et al., 2013; VanDeVelde et al., 2013; Garzione et al., 2014; Ji et al., 2018; Lechler et al., 2018; Zhai et al., 2019).

Paleosol-loess sequences contain various carbonate types (e.g., loess dolls, nodules, rhizoliths, land-snail shells, and earthworm biospheroliths) that are formed through a variety of processes that occur over different time periods (Zamanian et al., 2016a). All carbonate types that might be found in paleosol-loess sequences can be classified in three groups: (1) geogenic carbonates (i.e., "bulk" loess carbonates), which account for up to 30% of loess material; (2) biogenic carbonates, such as land-snail shells, earthworm biospheroliths, and micro mammal remains such as bones and teeth; and (3) pedogenic carbonates, such as rhizoliths, carbonate pendants, and nodules (Zamanian et al., 2016a). Formation of each carbonate type is governed by the same equilibrium equations:

$$CaCO_3 + H_2O + CO_2 \leftrightarrow Ca^{2+} + 2HCO_3^- \quad \text{(Eq. 1)}$$
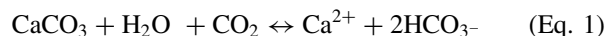
$$a_{CaCO_3} = \frac{4m_{Ca^{2+}}^3}{pCO_2}\left[\frac{K_2}{K_1 K_{cal} K_{CO_2}}\right] \quad \text{(Eq. 2)}$$

where calcite activity (α_{CaCO3}) varies as a function of the concentration of calcium ions in aqueous solution (m_{Ca}^{2+}), the partial pressure of CO_2 in the soil gas (pCO_2), and temperature-sensitive equilibrium constants for the dissociation of carbonic acid (K_1), bicarbonate (K_2), and calcite (K_{cal}), and for the hydration of CO_2 (K_{CO_2}) (Drever, 1982).

For each carbonate type, Equation 1 is driven to the left to cause $CaCO_3$ precipitation via distinct processes that operate over different time spans and locations (Zamanian et al., 2016a). In the case of biogenic carbonates, environmental conditions that promote (or restrict) biological activity, and growth must be considered. The mean lifespan of land-snails (depending on the species) is 3–5 years (Kerney and Cameron, 1979), and snails are more active at temperatures close to their growth optimum (Zaarur et al., 2011; Yanes et al., 2012). For example, the number of active *Arianta arbustorum* at 8°C is about five times higher than at 0°C and about two times higher than at 22°C (Cameron, 1970). *Pupilla muscorum* is active during the whole year, while the activity of *Succinella oblonga* is limited to the warm seasons of May to July (Pokryszko, 2001). In contrast, some pedogenic carbonates (e.g., rhizoliths) may form over a few

decades (Gocke et al., 2011). Pedogenic carbonate nodule and pendant formation takes place over hundreds to thousands of years (Gile et al., 1966; Birkeland, 1999) and occurs seasonally (Breecker et al., 2009), leading to clumped isotope temperatures that presumably reflect long-term averaged, and in many cases seasonally biased, environmental temperatures (Peters et al., 2013; Huntington and Lechler, 2015; Burgener et al., 2016; Gallagher and Sheldon, 2016; Gallagher et al., 2019; Huth et al., 2019; Kelson et al., 2020). The origin and time-integration of geogenic carbonate isotopic compositions may be more difficult to ascertain. Geogenic carbonates found in paleosol-loess sequences may record formation temperatures of minerals in the deflation area from which dust was sourced, where the minerals may have been formed through a variety of geological processes, including metamorphism (Catoni et al., 2012; Baez-Hernandez et al., 2019). Therefore, various carbonate types—even located in the same stratigraphic level in a paleosol-loess sequence—may record a mixture, but specific and potentially complementary environmental information based on differences in $\delta^{13}C$, $\delta^{18}O$, and Δ_{47} values.

We examine paleoenvironmental information recorded by carbonate types from a well-known paleosol-loess sequence, the Upper Pleistocene Nussloch paleosol-loess in the Rhine Valley of southwestern Germany (Zoller et al., 1988; Hatté et al., 1999; Rousseau et al., 2002, 2017a, b; Antoine et al., 2009; Prud'homme et al., 2018). Taken together, the $\delta^{18}O$, $\delta^{13}C$, and Δ_{47} data for multiple carbonate types enable us to investigate the effects of geogenic carbonate input, pedogenesis, and environmental factors on resulting isotopic variations.

MATERIALS AND METHODS

Study area and sampling

The Nussloch paleosol-loess sequence (49°18.82′N, 8°43.01′E) in southwestern Germany (Fig. 1a) is a well-studied type section of the European paleosol-loess. The Upper Pleniglacial sequence in Nussloch, with a total thickness of 18.5 m, has been dated by ^{14}C (Lang et al., 2003; Rousseau et al., 2007; Moine et al., 2017) and infrared-stimulated luminescence (Antoine et al., 2001, 2009), indicating formation throughout the last glacial-interglacial cycle since ~130 ka (Zoller et al., 1988; Hatté et al., 1998; Rousseau et al., 2007, 2017a). We sampled the younger part of the Nussloch sequence, which contains various morphologies of carbonates, including rhizoliths, loess dolls, land-snail shells, carbonate coatings, and hypocoatings, as well as concretions and earthworm biospheroliths (Moine et al., 2008, 2017; Gocke et al., 2011; Prud'homme et al., 2016, 2018).

Sampling focused on the most abundant carbonate morphologies (i.e., rhizoliths, loess doll, land-snail shells, and earthworm biospheroliths) from three horizons (Fig. 1b). The sampled horizons are: (1) ca. 20 ka loess unit at 5–6 m below the modern surface ("Upper loess"), (2) the ca. 38 ka paleosol (Lohne soil) at ~12 m below the modern surface
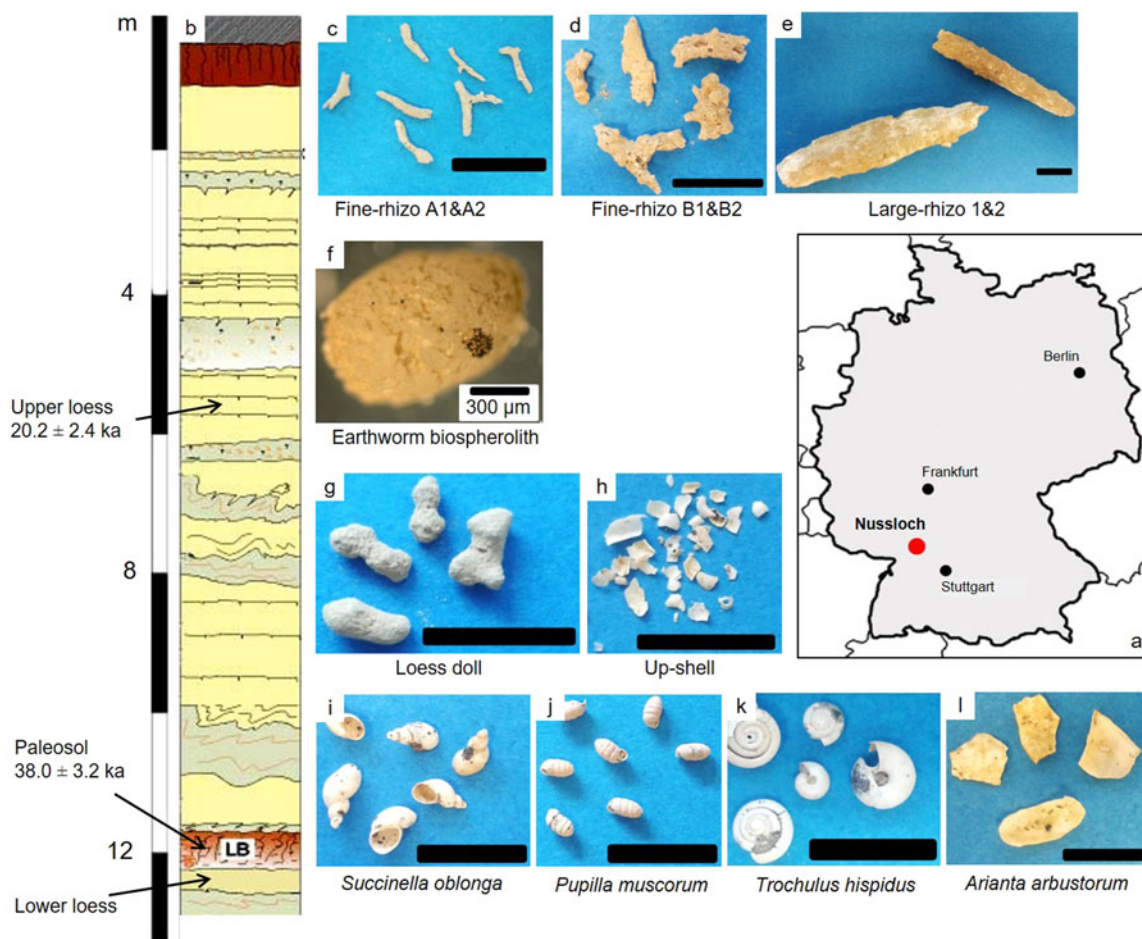
Figure 1. (color online) (a) The location of the Nussloch paleosol-loess sequence (49°18.82′N, 8°43.01′E) in southwestern Germany. (b) The sampling depths (adapted from Antoine et al., 2009) and (c–l) the types of carbonates collected from each depth. The black scale bar on all images is 1 cm, except (f) earthworm biospheroliths, which is 300 μm.

("Paleosol"), and (3) the loess unit directly below the paleosol ("Lower loess"). The sampled layers correspond to units 32 and 31, 20 and 19 described by Antoine et al. (2009), respectively. Bulk samples (∼10 kg each) were collected in the field from ∼50 cm deep into 1-m-wide outcrops that were freshly cleaned off by the authors. Bulk samples were taken to the lab and the various carbonate types were separated through wet sieving using a 50 μm screen. The following carbonate types were separated from each layer (Fig. 1c–l):

Upper loess: short and thin rhizoliths, < 1 mm in diameter and up to 1 cm long ("Fine-rhizo A;" Fig. 1c); short and thick rhizoliths, a few mm in diameter and length ("Fine-rhizo B;" Fig. 1d); large rhizoliths, up to 2 cm in diameter and 10 cm long ("Large-rhizo;" Fig. 1e); earthworm biospheroliths, average ∼1 mm in diameter (Fig. 1f); loess dolls, a few mm in diameter and < 1 cm long with different shapes (e.g., elongated ovals or globules with rounded edges; Fig. 1g); a few small white shell pieces of unidentified taxa with a maximum length of 5 mm ("Up-shell;" Fig. 1h); and bulk loess (26% calcium carbonate equivalent; CCE).

Paleosol: Land-snail shells of *Succinella oblonga* (Fig. 1i), *Pupilla muscorum* (Fig. 1j), *Trochulus hispidus* (Fig. 1k), *Arianta arbustorum* (Fig. 1l), and bulk paleosol (21% CCE).

Lower loess: Land-snail shells of *Succinella oblonga* (Fig. 1i), *Pupilla muscorum* (Fig. 1j), *Trochulus hispidus* (Fig. 1k), *Arianta arbustorum* (Fig. 1l), and bulk loess (25% CCE). The land-snail shells observed and sampled in the Lower loess are the same species as those from the paleosol.

Stable isotope analysis and calculations

Carbonate samples were ground with a mortar and pestle into homogenized powders prior to stable isotope ($\delta^{18}O$, $\delta^{13}C$, Δ_{47}) analyses at the University of Washington IsoLab. Sample preparation and analysis followed methods of Burgener et al. (2016) and Schauer et al. (2016). Briefly, 8–20 mg of powdered carbonate was reacted in a common phosphoric acid bath held at 90°C. The released CO_2 was purified cryogenically through an automated nickel and stainless steel vacuum line using an ethanol-dry ice slush trap and liquid N_2 trap, then chromatographically with a helium carrier through a Porapak Q trap (50/80 mesh, 15 cm long, 4.5 mm ID, 0.635 mm OD, held at -20°C). Preparation was completed when the sample CO_2 was frozen into a 6 mm Pyrex tube and flame sealed. The break seal containing purified CO_2 was loaded on the

autosampler of a Thermo MAT 253 dual inlet mass spectrometer to measure mass to charge ratio (*m/z*) 44–49. The intra-laboratory carbonate standards of C64, C2, and Coral (referenced to VPDB using NBS19 and LSVEC for $\delta^{13}C$, and NBS19 and NBS18 for $\delta^{18}O$), as well as interlaboratory calcite standards ETH1-4 (Meckler et al., 2014; Bernasconi et al., 2018), were purified and analyzed following the same procedures as Nussloch samples. Two to eight replicates were analyzed per carbonate sample, based on available sample mass.

Δ_{47}, $\delta^{13}C$, and $\delta^{18}O$ values from mass spectrometer data were calculated based on Huntington et al. (2009) using the pressure baseline correction of He et al. (2012), with data reduction and ^{17}O correction methods and scripts from Schauer et al. (2016). Δ_{47} values were placed in the carbon dioxide equilibrium scale, or absolute reference frame (Dennis et al., 2011), using CO_2 gases heated to 1000°C or equilibrated with water at 4°C and 60°C. Peirce outlier tests (Ross, 2003) were applied to identify replicate outliers (4 of 75 Δ_{47} analyses [5%] identified as outliers based on either Δ_{47} or $\delta^{13}C$ value), following which mean Δ_{47} and standard error (S.E.) of the mean values were calculated. Standard error of the mean Δ_{47} value is calculated as the standard deviation (taken to be the standard deviation of the sample replicates or the long-term standard deviation of carbonate standards, whichever is larger) divided by the square root of the number of replicates. T(Δ_{47}) was calculated for mean Δ_{47} using the calibration of Petersen et al. (2019), which is based on data produced using the same or similar analytical methods and the same ^{17}O correction as our samples. $\delta^{13}C$ and $\delta^{18}O$ values were placed on the VPDB scale using C64 and C2 for $\delta^{13}C$, and C64 and coral for $\delta^{18}O$.

To calculate the oxygen isotopic composition of the water from which the carbonate precipitated ($\delta^{18}O_{water}$), the equations in Kim and O'Neil (1997) were used to calculate the temperature-dependent fractionation factor α for calcite and aragonite (Eqs. 3, 4).

$$1000 \ln \alpha \text{ (Calcite-H}_2\text{O)} = 18.03 \times (10^3 T^{-1}) - 32.42$$
$$\text{(Eq. 3)}$$

$$1000 \ln \alpha \text{ (Aragonite-H}_2\text{O)} = 17.88 \times (10^3 T^{-1}) - 31.14$$
$$\text{(Eq. 4)}$$

To estimate α for shell carbonates comprising both aragonite and calcite (shells contained 62–100% aragonite; determined by the authors), we did a mass balance of the two relationships. The $\delta^{18}O_{water}$ was then calculated based on Eq. 5:

$$\delta^{18}O_{water} = (\delta^{18}O_{carbonate} + 1000)/(\alpha - 1000) \quad \text{(Eq. 5)}$$

RESULTS

Isotopic results for Upper loess, Paleosol, and Lower loess samples are summarized in Table 1, and full data for samples and standards is provided in Supplementary Table A1.

$\delta^{13}C$ and $\delta^{18}O$ of carbonate types

Carbonate $\delta^{13}C$ values ranged from -11 to -0.5‰ and $\delta^{18}O$ values from -6.1‰ to -2.2‰ (VPDB), with the average uncertainties of individual measurements of 0.04‰ and 0.03‰ for $\delta^{13}C$ and $\delta^{18}O$, respectively.

All rhizoliths, loess dolls, and bulk loess samples in the Upper loess have similar carbonate $\delta^{18}O$ values ranging from -6.1 to -5.6‰ (VPDB). $\delta^{18}O$ values of shell samples and earthworm biospheroliths from this horizon are significantly higher at -2.3 and -4.7‰, respectively (VPDB) (Table 1, Fig. 2). While all Upper loess rhizoliths have similar $\delta^{18}O$ values (-5.9 ± 0.1‰ VPDB, ± 1σ, n = 22), $\delta^{13}C$ values depend on rhizolith size. Small rhizoliths (Fine-rhizo A and B) have average $\delta^{13}C$ values (-6.1 ± 0.4‰) that are 2‰ higher than Large-rhizo samples from this interval (-7.0‰ and -8.2‰). $\delta^{13}C$ values for the shell sample (-6.6‰) and pedogenic loess dolls (~-7.0‰) from the Upper loess fall within the range of rhizoliths from this horizon. Earthworm biospheroliths from the Upper loess are characterized by the lowest $\delta^{13}C$ for the interval at -11.5 ‰. Measured $\delta^{13}C$ for bulk loess in the Upper loess interval (-0.5‰) is significantly higher than all other carbonates from the same horizon, a relationship consistently observed in the other sampled horizons.

The Lower loess and Paleosol samples show similar shifts in $\delta^{13}C$ and $\delta^{18}O$ values by carbonate type, with the shells having significantly lower $\delta^{13}C$ and higher $\delta^{18}O$ values than the bulk loess or bulk paleosol. The three sampled shell species *S. oblonga*, *P. muscorum*, and *T. hispidus* in the Lower loess and the Paleosol have a narrow and similar range of $\delta^{18}O$ values (-3.8 ± 0.2‰), which is more than 1‰ lower than values for *A. arbustorum* (-2.3 ± 0.1‰). The $\delta^{13}C$ values of *S. oblonga*, *P. muscorum*, and *T. hispidus* sampled in both horizons (-3.1‰ to -6.1‰) are systematically offset relative to $\delta^{13}C$ values of the bulk paleosol (-1.9‰) and bulk loess from the Lower loess interval (-0.9‰) (Fig. 2). $\delta^{13}C$ values for *A. arbustorum* are similar across the Paleosol and Lower loess horizons (-8‰). A similar magnitude $\delta^{13}C$ offset is observed for bulk loess/paleosol carbonate samples from the Lower loess and Paleosol horizons (Fig. 2).

Formation temperatures [T(Δ_{47})] of carbonate types

Measured carbonate Δ_{47} values range from 0.754–0.499‰, corresponding to apparent temperatures of 8–120°C (Table 1). The T(Δ_{47}) values of the bulk carbonate samples range from ~78–120°C, far exceeding Earth-surface temperature conditions, while T(Δ_{47}) values for other carbonate types (i.e., pedogenic and biogenic) range from ~8–38°C and are in the plausible range of Earth-surface temperatures (Fig. 3). The small rhizoliths (Fine-rhizo A and B) in the Upper loess (Fig. 3) yielded temperatures of 24 ± 4°C and 30 ± 2°C, respectively, one of which is indistinguishable from loess doll T(Δ_{47}) (23 ± 3°C). The small rhizolith and loess doll temperatures are distinguishable from the temperatures of two Large-rhizo samples (12 ± 4 and 15 ± 5°C),

Table 1. Stable isotopes and clumped isotope data for carbonate types collected from three depths at Nussloch paleosol-loess sequence.

								Replicate analyses					Sample averages and external error (SE)					T (°C)	±1SE	Aragonite	Calcite	δ¹⁸O		δ¹⁸O water ‰
Carbonate materials		Sample ID	$\delta^{13}C$ ‰VPDB	$\delta^{13}C$ Std. mass spec	$\delta^{18}O$ ‰VPDB	$\delta^{18}O$ Std. mass spec.	Δ_{47} ‰VPDB	Δ_{47} SE. mass spec	Average $\delta^{13}C$ ‰	$\delta^{13}C$ SE.	average $\delta^{18}O$ ‰	$\delta^{18}O$ SE.	average Δ_{47} ‰	Δ_{47} SE	Petersen et al. (2019)	analytical	%	%	(VSMOW)	α	VPDB
Upper loess	Up-shell	160912_1_1	−6.632	0.004	−2.318	0.006	0.713	0.009	−6.647	0.015	−2.306	0.012	0.732	0.019	12	6	100	0.0	28.533	1.032	−3.399
		160922_1_1	−6.661	0.004	−2.294	0.009	0.752	0.008													
	Earthworm biospherolith	181115_1_ULewrm	−11.378	0.006	−4.747	0.010	0.716	0.010	−11.476	0.006	−4.722	0.012	0.745	0.011	8	3			26.042	1.032	−5.967
		181115_4_ULewrm	−11.420	0.006	−4.698	0.010	0.723	0.010													
		181227_4_ULewrm	−11.551	0.006	−4.685	0.012	0.729	0.009													
		181227_6_ULewrm	−11.556	0.006	−4.760	0.017	0.739	0.010													
	loess doll	160912_2_2	−7.020	0.004	−5.508	0.007	0.659	0.008	−6.977	0.014	−5.584	0.061	0.699	0.019	23	7			25.154	1.029	−3.586
		160922_2_2	−6.997	0.005	−5.483	0.009	0.745	0.009													
		160926_3_2	−6.950	0.004	−5.465	0.006	0.746	0.008													
		161006_1_2	−6.972	0.004	−5.743	0.009	0.666	0.008													
		161011_1_2	−6.945	0.004	−5.720	0.007	0.681	0.009													
	Fine-rhizo B1	160912_3_3	−5.663	0.004	−5.974	0.008	0.710	0.008	−5.789	0.004	−5.940	0.007	0.674	0.013	32	5			24.787	1.027	−2.106
		160922_3_3	−5.776	0.006	−5.748	0.009	0.698	0.008													
		161007_2_3	−5.906	0.004	−5.970	0.005	0.644	0.008													
		161011_2_3	−5.810	0.004	−6.067	0.007	0.645	0.009													
	Fine-rhizo B2	181228_4_ULfinerhizoB	−6.658	0.006	−5.904	0.011	0.680	0.009	−6.609	0.006	−5.870	0.014	0.689	0.012	27	5			24.858	1.028	−3.098
		181228_6_ULfinerhizoB	−6.624	0.006	−5.915	0.014	0.665	0.012													
		190107_4_finerhizoB	−6.546	0.006	−5.792	0.016	0.667	0.009													
	Large-rhizo 1	*160920_1_4**	−7.275	0.004	−6.177	0.007	0.670	0.008	−7.079	0.004	−6.128	0.007	0.725	0.016	15	5			24.610	1.031	−5.923
		160922_4_4	−7.028	0.006	−6.064	0.008	0.736	0.009													
		160926_6_4	−6.942	0.003	−6.040	0.007	0.745	0.008													
		161012_1_4	−7.069	0.004	−6.231	0.007	0.693	0.009													
	Large-rhizo 2	181115_2_ULlgrhizo	−8.114	0.007	−6.060	0.010	0.717	0.010	−8.195	0.006	−6.017	0.014	0.733	0.012	12	4			24.716	1.031	−6.397
		181227_5_ULlgrhizo	−8.232	0.006	−6.041	0.015	0.734	0.011													
		*181227_7_Ullgrhizo**	−8.223	0.006	−6.043	0.010	0.813	0.010													
		190107_1_ULlgrhizo	−8.212	0.007	−5.925	0.020	0.693	0.011													
	Fine-rhizo A1	160912_6_5	−5.695	0.005	−6.043	0.007	0.706	0.008	−5.769	0.004	−6.004	0.007	0.712	0.012	19	4			24.720	1.030	−4.958
		160922_6_5	−5.547	0.004	−5.796	0.008	0.698	0.008													
		160926_7_5	−6.064	0.004	−6.174	0.006	0.734	0.008													
	Fine-rhizo A2	181227_8_ULfinerhizoA	−6.237	0.006	−5.771	0.010	0.679	0.010	−6.217	0.006	−5.711	0.012	0.685	0.014	28	5			25.023	1.028	−2.645
		181228_3_ULfinerhizoA	−6.249	0.006	−5.724	0.009	0.695	0.010													
		181228_5_ULfinerhizoA	−6.168	0.005	−5.732	0.010	0.660	0.008													
		190107_2_finerhizoA	−6.212	0.007	−5.618	0.019	0.633	0.010													
	bulk loess	160909_1_20	−0.446	0.004	−5.545	0.007	0.568	0.008	−0.497	0.064	−5.590	0.104	0.558	0.012	91	8			25.147	1.017	7.768
		160926_1_20	−0.624	0.004	−5.437	0.005	0.566	0.008														
		161005_1_20	−0.420	0.004	−5.789	0.007	0.538	0.009														

(*Continued*)

Table 1. Continued.

Carbonate materials		Sample ID	Replicate analyses						Sample averages and external error (SE)						T (°C) Petersen et al. (2019)	±1SE analytical	Aragonite	Calcite	δ18O (VSMOW)	α	δ18O water ‰ VPDB
			δ13C ‰VPDB	δ13C Std. mass spec	δ18O ‰VPDB	δ18O Std. mass spec.	Δ47 ‰VPDB	Δ47 SE. mass spec	Average δ13C ‰	δ13C SE.	average δ18O ‰	δ18O SE.	average Δ47 ‰	Δ47 SE			%	%			
Paleosol	*Succinella oblonga*	160912_7_6*	−4.020	0.004	−4.043	0.008	0.739	0.009	−4.128	0.004	−4.021	0.007	0.661	0.011	38	4	62.6	37.4	26.765	1.026	+0.298
		161003_1_6	−4.115	0.004	−3.953	0.007	0.678	0.007													
		161007_4_6	−3.961	0.004	−4.170	0.007	0.654	0.008													
		161011_4_6	−4.307	0.004	−4.033	0.006	0.663	0.011													
		161012_2_6	−4.130	0.005	−3.928	0.007	0.649	0.010													
		*190128_1_Paleosol_Soblonga**	−4.798	0.007	−3.653	0.016	0.681	0.011													
	Pupilla muscorum	160920_2_7	−5.834	0.013	−3.564	0.023	0.704	0.010	−6.146	0.008	−3.544	0.015	0.720	0.018	16	6	100	0.0	27.257	1.031	−3.805
		160923_2_7	−6.396	0.005	−3.321	0.011	0.739	0.010													
		161003_2_7	−5.869	0.005	−3.644	0.007	0.718	0.009													
		190128_2_Paleosol_Pmuscorum	−6.485	0.007	−3.646	0.018	0.701	0.010													
	Trochulus hispidus	160913_2_8	−5.816	0.005	−3.824	0.005	0.699	0.007	−5.752	0.052	−3.788	0.108	0.687	0.012	27	5	75.6	24.4	27.005	1.029	−1.517
		160923_3_8	−5.792	0.005	−3.586	0.006	0.673	0.008													
		161003_3_8	−5.648	0.004	−3.954	0.006	0.690	0.008													
	Arianta arbustorum	160913_4_9	−8.100	0.004	−2.440	0.006	0.724	0.007	−8.128	0.028	−2.395	0.025	0.732	0.012	12	4	89.4	10.6	28.441	1.032	−3.395
		160923_4_9	−8.101	0.005	−2.352	0.006	0.718	0.009													
		161003_4_9	−8.183	0.004	−2.393	0.006	0.754	0.007													
	bulk paleosol	160909_2_21	−1.918	0.004	−5.325	0.009	0.573	0.008	−1.865	0.030	−5.314	0.032	0.578	0.012	78	7			25.431	1.019	6.260
		160921_3_21	−1.860	0.004	−5.254	0.008	0.578	0.007													
		161005_2_21	−1.816	0.006	−5.363	0.011	0.582	0.008													
Lower loess	*Succinella oblonga*	160913_5_10	−2.976	0.003	−4.052	0.007	0.672	0.007	−3.152	0.005	−3.805	0.010	0.665	0.014	36	6	62.6	37.4	26.987	1.027	0.237
		160923_6_10	−2.867	0.004	−3.927	0.008	0.699	0.008													
		161004_1_10	−3.085	0.005	−3.994	0.009	0.628	0.008													
		190128_5_LowLoessSoblonga	−3.501	0.007	−3.611	0.019	0.622	0.011													
		190926_5_LowLoess_Soblonga	−3.332	0.005	−3.442	0.006	0.701	0.006													
	Pupilla muscorum	160913_6_11	−4.384	0.004	−4.090	0.007	0.736	0.007	−4.759	0.005	−3.724	0.010	0.706	0.012	21	4	100	0.0	27.071	1.030	−2.955
		161004_2_11	−4.408	0.006	−4.118	0.010	0.694	0.009													
		190128_4_LowLoessPmusc	−5.199	0.006	−3.573	0.018	0.677	0.010													
		191031_2_LowLoessPmusc	−4.875	0.004	−3.429	0.007	0.701	0.006													
		191031_3_LowLoessPmusc	−4.930	0.004	−3.409	0.007	0.731	0.006													
	Trochulus hispidus	160920_3_12	−4.846	0.005	−3.828	0.009	0.667	0.009	−4.610	0.005	−3.800	0.009	0.674	0.012	32	5	75.6	24.4	26.993	1.028	−0.570
		160922_7_12	−4.476	0.004	−3.645	0.008	0.689	0.006													
		161004_3_12	−4.507	0.005	−3.926	0.009	0.668	0.010													
	Arianta arbustorum	190926_1_LowLoess_shell	−7.968	0.005	−2.167	0.007	0.742	0.006	−7.957	0.005	−2.218	0.007	0.723	0.011	15	3	89.4	10.6	28.623	1.031	−2.588
		190926_3_LowLoess_shell	−7.939	0.004	−2.232	0.006	0.753	0.007													
		190926_4_LowLoess_shell	−7.920	0.005	−2.261	0.007	0.727	0.007													
		191031_4_LowLoessShell	−8.002	0.005	−2.213	0.007	0.734	0.007													
	bulk loess	160921_4_22	−1.791	0.004	−5.101	0.008	0.499	0.008	−0.864	0.463	−5.441	0.210	0.518	0.012	120	10			25.300	1.013	11.662
		161005_3_22	−0.400	0.004	−5.648	0.011	0.536	0.008													
		161007_3_22	−0.402	0.005	−5.575	0.007	0.518	0.008													

* Outliers are noted in italics

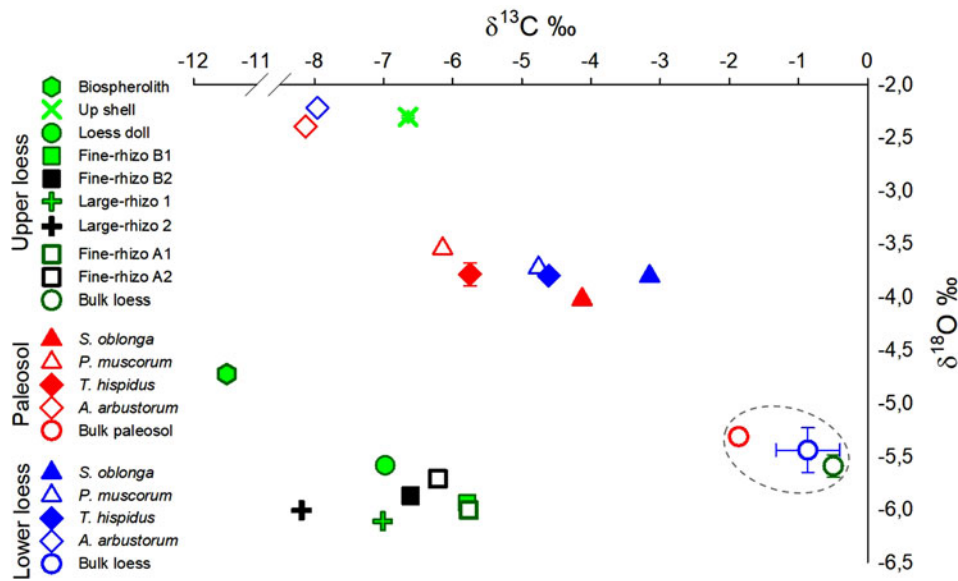**Figure 2.** (color online) Isotopic composition of carbon (δ^{13}C) and oxygen (δ^{18}O) in various carbonate types present in the three sampled horizons in the Nussloch paleosol-loess sequence. The δ^{13}C and δ^{18}O in bulk loess carbonates is indicated by the grey-dashed circle. Note the shift (-1‰) in δ^{13}C values of land-snail *S. oblonga*, *P. muscorum*, and *T. hispidus* shells from Lower loess to Paleosol. A similar magnitude δ^{13}C shift is observed between δ^{13}C values of bulk carbonates from Lower loess to Paleosol. Where errors are larger than the size of the symbols, standard errors are shown with horizontal and vertical bars, respectively, for δ^{13}C and δ^{18}O.

Up-shell (12 ± 6°C), and earthworm biospherolith (8 ± 3°C) samples. Land-snail shells revealed two distinct temperature ranges in both the Paleosol and the Lower loess horizons (Fig. 3). The clumped isotope temperatures for *S. oblonga* (38 ± 4 and 36 ± 6°C) and *T. hispidus* (27 ± 5 and 32 ± 5°C) are consistently warmer than analyzed *P. muscorum* (16 ± 6 and 21 ± 4°C) and *A. arbustorum* (12 ± 4 and 15 ± 3°C)

samples. Similar land-snail species show similar temperatures in the Paleosol and in the Lower loess (Fig. 3).

The calculated value of reconstructed δ^{18}O$_{water}$

Calculated apparent δ^{18}O$_{water}$ values vary among carbonate types (Fig. 4). Apparent δ^{18}O$_{water}$ for bulk loess and paleosol
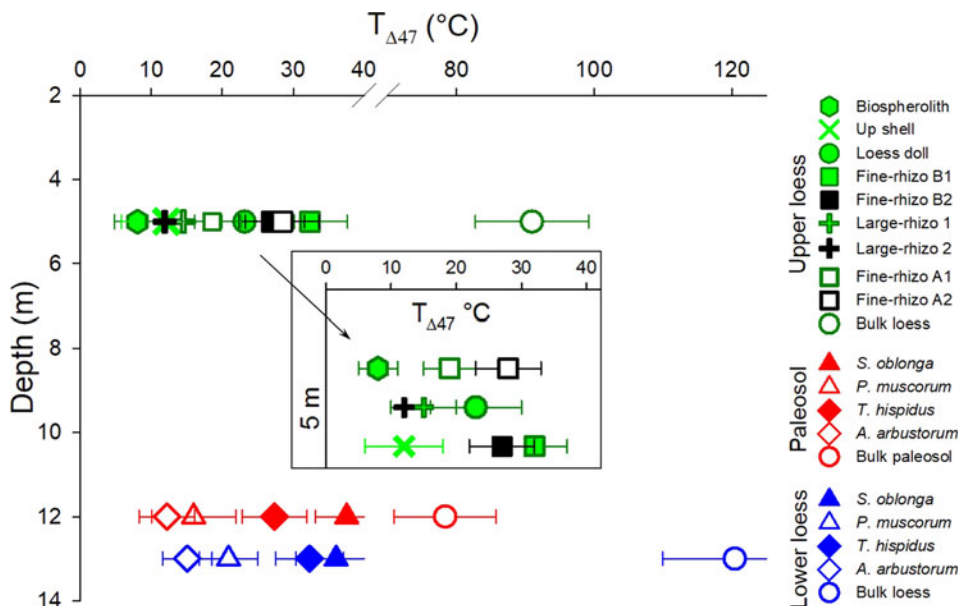
Figure 3. (color online) Temperature of carbonate formation calculated based on T(Δ_{47}) values of carbonate types present at three depths in the Nussloch paleosol-loess sequence. The inset graph shows the temperatures of carbonate types in the Upper loess horizon. Horizontal bars show standard errors.
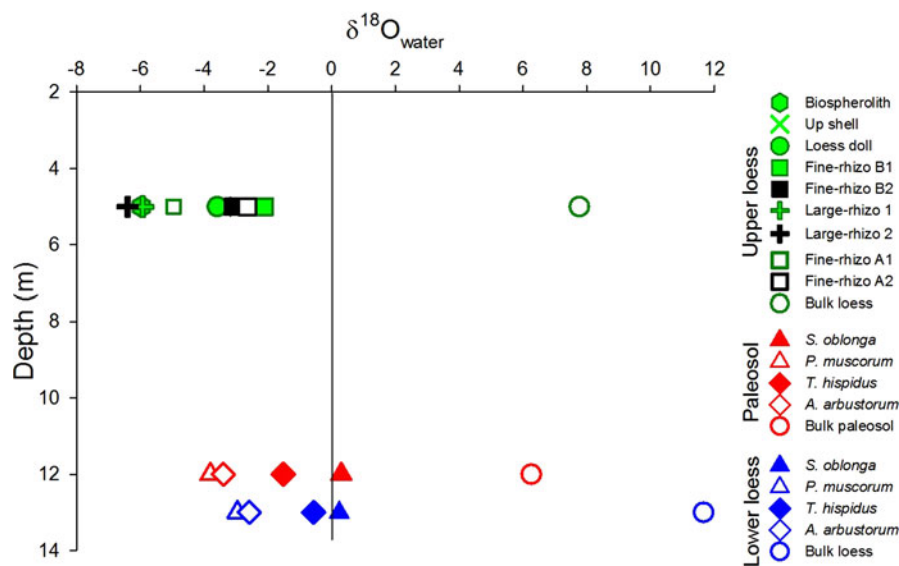
Figure 4. (color online) The estimated isotopic composition of water ($\delta^{18}O_{water}$), from which the carbonate types were formed. The error bars are smaller than the symbol size for all carbonate types. The solid vertical line at $\delta^{18}O_{water} = 0$ is shown for reference.

carbonates are positive values (6–12‰ VSMOW). In contrast, the other carbonate types (i.e. pedogenic and biogenic carbonates) have $\delta^{18}O_{water}$ values in the range of possible paleoenvironmental water values. Reconstructed apparent $\delta^{18}O_{water}$ values for rhizoliths of different sizes (-6.4 to -2.1‰), land-snail shells of different species (-3.8 to +0.3‰) and earthworm biospheroliths (-6.0‰) differ significantly, even at a similar depth. However, similar species of land-snails record similar reconstructed $\delta^{18}O_{water}$ values independent of depth (Fig. 4).

DISCUSSION

Stable isotopic compositions vary with carbonate type within a single sedimentological layer within the Nussloch loess-paleosol sequence. $T(\Delta_{47})$ in excess of 78°C indicates bulk loess and bulk paleosol carbonates are not suitable for paleoenvironmental reconstructions. In contrast, the pedogenic and biogenic carbonate types record distinct paleoenvironmental information, with sample $\delta^{18}O$, $\delta^{13}C$, and Δ_{47} values likely reflecting specific formation mechanisms and time periods over which the carbonates precipitated.

Geogenic carbonates: bulk loess and bulk paleosol samples

$\delta^{13}C$, $\delta^{18}O$, and $T(\Delta_{47})$ values suggest carbonates in bulk loess and bulk paleosols of the Nussloch sequence are detrital rather than pedogenic in origin. Apparent $T(\Delta_{47})$ values of bulk carbonates (~78–120°C) far exceed the range of plausible Earth-surface temperatures (Fig. 3). Additionally, calculated apparent $\delta^{18}O_{water}$ values of bulk carbonates (6.3–12‰; Fig. 4) are inconsistent with formation in situ in the (paleo)soil unit. Instead, the isotopic data point to

diagenetic and/or metamorphic sources for these carbonates, which we suggest were likely derived from pre-existing rock through processes of weathering and erosion.

Waters in metamorphic environments are commonly characterized by high $\delta^{18}O$ values (potentially > 0‰ VSMOW) as a result of dehydration processes and water-rock isotopic exchange in deep-crustal environments (Sheppard, 1986), which may explain the positive $\delta^{18}O_{water}$ values calculated for many bulk carbonates in the Nussloch sequence. Diagenetic and metamorphic carbonates are exposed throughout Western Europe, making it difficult to ascertain the exact source(s) of Nussloch detrital carbonate. That said, prevailing westerly and north-westerly winds into the Nussloch region during the last glacial period (Antoine et al., 2013; Rousseau et al., 2014) point to source regions to the west of the Nussloch Basin, possibly marbles exhumed in the Scottish Highlands and abundant limestone throughout the Devon Basin in England. Additional geochemical data (e.g., Sr-Nd isotopes) could potentially help decipher source(s) for Nussloch detrital carbonate. Nevertheless, high apparent $T(\Delta_{47})$ and $\delta^{18}O_{water}$ values of bulk carbonates indicate that bulk carbonates do not record the local environmental conditions during or following sedimentation and cannot be used as a direct paleoenvironmental proxy.

Pedogenic carbonates: rhizoliths and loess dolls

Rhizoliths and loess dolls are pedogenic carbonates formed in situ in the soil (e.g., Gocke et al., 2010, 2011; Li et al., 2015; Gao et al., 2020; Sun et al., 2020). Their $\delta^{13}C$ values should largely reflect vegetation type, their $\delta^{18}O_{water}$ mirror the values of local soil water, and $T(\Delta_{47})$ is presumably a measure of the soil temperature during soil drying and CO_2 degassing. The pedogenic carbonate isotopic values are generally

consistent with formation in soil conditions. In the following paragraphs, we examine the pedogenic carbonate data in the context of the range of $\delta^{13}C$, $\delta^{18}O$, and $T(\Delta_{47})$ values expected for Nussloch site paleoenvironmental conditions and discuss implications of distinct seasonality and mechanisms of pedogenic carbonate formation for paleoenvironmental reconstruction.

Multiple lines of evidence place constraints on Nussloch paleoenvironmental conditions relevant to the period of pedogenic carbonate formation. We lack direct constraints on local terrestrial $\delta^{18}O_{water}$ values during this period; however, Sima et al. (2009) assumed that precipitation sources and dominant wind trajectories were similar to modern during the Last Glacial. Such $\delta^{18}O_{water}$ values of precipitation would differ by only ~0.5‰ from modern (-11‰ to -7‰) (Field, 2010; Terzer et al., 2013) due to the ice volume effect (Prud'homme et al., 2016). Today, minimum and maximum monthly mean air temperatures in the study area range from ~0 to ~25°C, and average cold- and warm-season air temperatures are $1.7 \pm 0.9°C$ (DJF) and $18 \pm 2°C$ (JJA), respectively. The mean annual air temperature is 10°C, and modern mean annual soil temperature is therefore likely to be in the range of 10°C to up to 3–5°C higher due to radiative heating of the soil surface (Roxy et al., 2014). Significant elevation of soil surface temperatures via radiative heating is common when the annual precipitation is < 600 mm (Burgener et al., 2019; Gallagher et al., 2019), as it is estimated to have been in Nussloch (Prud'homme et al., 2018). Recent air and soil temperature estimates from earthworm calcite granules at Nussloch suggest similar-to-modern mean warm season air and soil temperatures of 12 ± 4 and $15 \pm 5°C$, respectively, during paleosol formation (Prud'homme et al., 2016). These temperature estimates were based on measured carbonate $\delta^{18}O$ and assumed $\delta^{18}O_{water}$ values for the Nussloch paleosol-loess sequence. Other paleo-temperature estimates suggest comparable-to-modern mean annual air temperatures of 8.5–10°C during paleosol formation in analogous paleosol-loess sequences in Hungary (Schatz et al., 2015).

Within these ranges of temperature, the season over which the rhizoliths are formed and the formation mechanisms of rhizoliths should determine the isotopic values and temperatures recorded. Nussloch rhizolith samples have $\delta^{13}C$ values that are dependent on rhizolith size: small rhizoliths have higher $\delta^{13}C$ values than large rhizoliths and loess dolls from the same horizon (Fig. 2). We interpret the dependence of the $\delta^{13}C$ values with rhizolith size to suggest that these carbonates originate from different plant species or groups, and/or form through specific mechanisms (e.g., root water uptake or soil wetting-drying cycles), motivating hypotheses that can be tested using the suite of $\delta^{13}C$, $\delta^{18}O$ and $T(\Delta_{47})$ data.

First, it is possible that rhizolith formation mechanisms vary with time. Water uptake by roots and resulting water flow toward the root is accepted as the main formation mechanism for rhizoliths (Klappa, 1980; Lambers et al., 2009; Gocke et al., 2011). Following root death, water uptake by the root and water flow towards the root is stopped. However, non-biogenic mechanisms (e.g., wetting-drying cycles) can still drive further carbonate dissolution and precipitation. In this way, a rhizolith formed in association with water uptake by roots may subsequently act as a framework for further carbonate precipitation to build on such that increased size of the rhizolith records a longer formation period (Sun et al., 2019b, c; Huguet et al., 2020). In this scenario, specific formation mechanisms operating over different time scales would affect the environmental information recorded by rhizoliths larger than a few millimeters compared to smaller rhizoliths that presumably form over a short period of time associated with active root water uptake.

Vegetation type could also cause differences in the isotopic signals recorded by large and small rhizoliths. Indeed, a variety of vegetation species are associated with rhizolith formation (Rodriguez-Aranda and Calvo, 1998; Alonso-Zarza, 1999; Matteucci et al., 2007). If large rhizoliths form along perennial roots that are bigger than the roots of annual grasses, this would lead to continued root-water uptake over many years. In contrast, the morphology of small rhizoliths suggest that they formed along the smaller roots of annual grasses, likely over one growing season. Such a difference in duration of carbonate formation could explain the observed differences in $\delta^{13}C$, $\delta^{18}O$, and $T(\Delta_{47})$ values among large and small rhizoliths. Alternatively, small rhizoliths might have formed when the plant was under water stress, for example at the end of the winter season through the early spring (Tranquillini, 1982), which is most probably the case in glacial times (Yung et al., 1996; Medeiros and Ward, 2013). Under such conditions the plant will close the stomata to reduce water loss, which leads to ^{13}C enrichment by C3 photosynthesis (e.g., Dawson et al., 2002). Observed differences in temperature and $\delta^{18}O_{water}$ values among small versus large rhizoliths could be consistent with small-rhizolith formation under water stress, with fine rhizoliths recording higher formation temperature (Fig. 3) and forming from more evaporative waters (Fig. 4). The $\delta^{13}C$ values (Fig. 2) do not show obvious evaporation control, potentially reflecting other factors, such as plant type, that may influence $\delta^{13}C$ values.

We suggest that rhizolith formation temperatures (Fig. 3) are consistent with differences in formation duration and mechanisms. We suggest small rhizoliths likely formed over short periods, potentially as short-lived as during a single soil-drying event due to root-water uptake. In contrast, large rhizoliths may have formed over a few years up to a few decades (Gocke et al., 2011; Sun et al., 2019a) integrating several warm seasons, and therefore recording the mean temperature of those seasons. We therefore interpret the clumped isotope temperature for the large rhizoliths (average $T[\Delta_{47}] = 14 \pm 5°C$) to represent warm-season soil conditions averaged over up to a few decades.

The clumped isotope warm-season soil temperature reconstruction is consistent with the average mean warm-season soil temperature estimates ($13 \pm 4°C$ and $15 \pm 3°C$) reported for Nussloch (Prud'homme et al., 2016, 2018). Prud'homme et al. (2016) estimated $\delta^{18}O_{water}$ values during last glacial at Nussloch based on a linear equation among modern values of water $\delta^{18}O$ ($\delta^{18}O_{mwater}$) and modern mean annual air
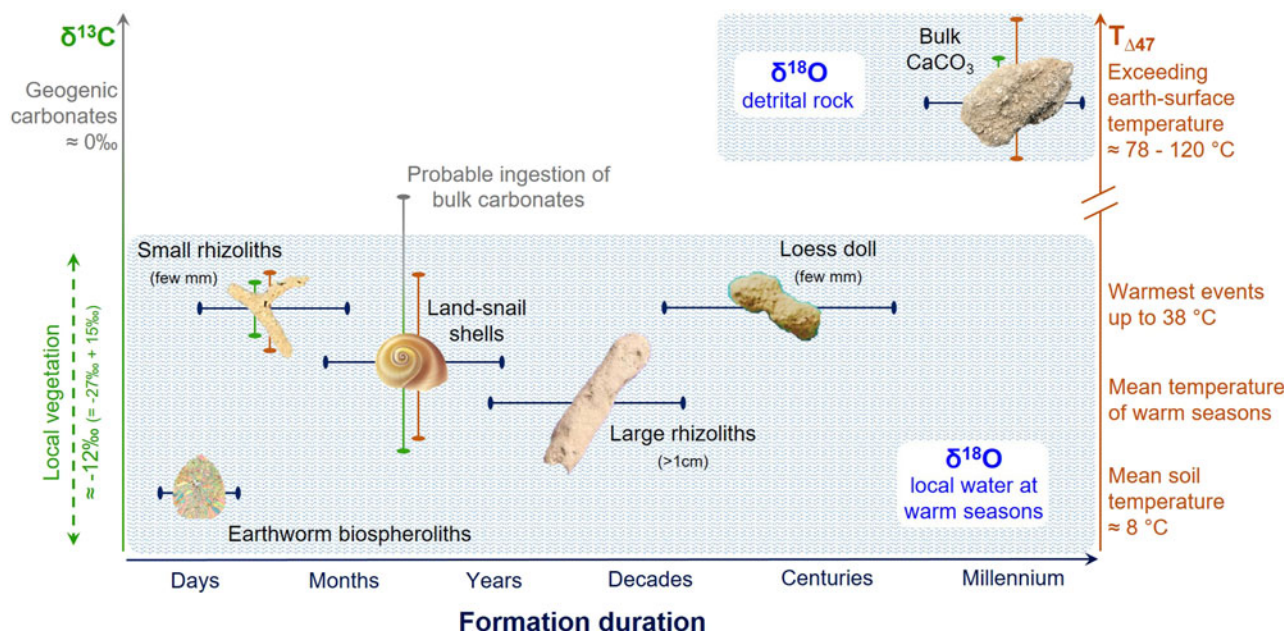
Figure 5. (color online) Dependency and resolution of paleoenvironmental interpretations based on carbonate types on formation duration and formation mechanisms. While $\delta^{13}C$ and $T(\Delta_{47})$ are plotted on the left and right y-axes, respectively, $\delta^{18}O$ is lumped into the two pools and shown as the two blue shaded regions. While bulk carbonates show more positive $\delta^{13}C$ values of geogenic origins (~0‰), pedogenic and biogenic carbonates record $\delta^{13}C$ values of local vegetation. Note that the $\delta^{13}C$ values of local vegetation (~ -27‰ for C3 species) are enriched by about 15‰ during carbonate precipitation process (e.g., -12‰ for earthworm biospheroliths). Some error bars are smaller than the symbols.

temperature of the IAEA dataset, and used the $\delta^{18}O_{mwater}$ values to calculate temperature from carbonate $\delta^{18}O$. Assuming measured $T(\Delta_{47})$ values record soil carbonate formation temperatures, we can directly calculate the $\delta^{18}O_{water}$ values during rhizolith formation. The good agreement between temperature results from our study and those of Prud'homme et al. (2016) suggest that the assumptions by Prud'homme et al. (2016) about paleo $\delta^{18}O_{water}$ values at Nussloch during the last glacial interval were reasonable.

Loess doll formation may occur over centuries or longer depending on size (Zamanian et al., 2016a), rather than during a single vegetation period like small rhizoliths. However, the loess dolls and one of the small rhizolith samples are similar in both formation temperatures and size (Figs. 1, 3). Thus, it is possible that the small loess dolls might also be formed over short periods, although more evidence than just formation temperature would be necessary to substantiate such an argument.

Taken together with the $\delta^{13}C$ and $\delta^{18}O$ data, $T(\Delta_{47})$ values further support interpretation of differences in duration of carbonate growth by carbonate type (Fig. 5). We suggest that small rhizoliths (a few millimeters in diameter) and loess dolls exhibiting large variability in $T(\Delta_{47})$ (19–32°C) record the temperature of one growing season and/or soil-drying event. Such transient growth during peak warm-season events can explain why observed $T(\Delta_{47})$ values are significantly warmer than expected for growth during glacial conditions. In contrast, we interpret average $T(\Delta_{47})$ of ~14°C for large rhizoliths (a few centimeters in diameter) as a more reliable measure of average paleo-temperatures across multiple growing seasons, or over decades (Table 1, Fig. 3).

Biogenic carbonates: land-snail shells and earthworm biospheroliths

The $\delta^{13}C$ and $\delta^{18}O$ values of distinct land-snail species (Fig. 2) reflect the specifics in the diet of these organisms (i.e., ingested plants and, to a lesser extent, geogenic carbonate). $\delta^{13}C$ values in shell carbonate depend mainly on the land-snail diet regime (Metref et al., 2003; Balakrishnan et al., 2005; Zhang et al., 2014). The similar shift (~ -1‰) to lower $\delta^{13}C$ values from Lower loess to paleosol in both land-snail shells and bulk carbonates reveals that the land snails *S. oblonga*, *P. muscorum*, and *T. hispidus* were ingesting bulk carbonate (Pigati et al., 2010; Yanes et al., 2012) (Fig. 2). These identified species are all able to ingest carbonates (Fechter et al., 1990; Boschi et al., 2011), which comprise ~5–25% of their diet (Pigati et al., 2010; Yanes et al., 2012). We can estimate the $\delta^{13}C$ of vegetation during paleosol formation and Lower loess deposition using the equation of Yanes et al. (2008) based on shell carbonate $\delta^{13}C$ values. Using this equation, and assuming 0% carbonate ingestion, the range of $\delta^{13}C$ of vegetation is calculated as -22 to -17‰ VPDB; but considering 5–25% carbonate ingestion, the estimated $\delta^{13}C$ values of vegetation range from -25‰ to -20‰ VPDB. The latter calculated $\delta^{13}C$ range of vegetation is consistent with the reported $\delta^{13}C$ values of organic carbon (-24.9 to -23.7‰) for the Nussloch paleosol-loess sequence (Hatté et al., 1999; Prud'homme et al., 2018), supporting our interpretation of significant carbonate ingestion by analyzed snail species. Similar calculations using *A. arbustorum*, which we assume did not ingest carbonate due to the similarity of $\delta^{13}C$ values for co-occurring shell and non-biogenic carbonate in

paleosol and Lower loess, also gives a $\delta^{13}C$ value of -26‰ for vegetation. Lastly, earthworm biospheroliths also can be used to reconstruct plant $\delta^{13}C$ (Prud-hommme et al., 2018). Using an epsilon calculated from Canti (2009) and typical diet estimation equations (Passey et al., 2005), we calculate a $\delta^{13}C_{plant}$ of -23‰ from the earthworm biospheroliths $\delta^{13}C$ values.

The clumped isotope data and calculated $\delta^{18}O_{water}$ values are broadly consistent with the hypothesis that land-snail individuals record seasonal and local changes in atmospheric temperature (Eagle et al., 2013; Wang et al., 2016; Zhang et al., 2018; Zhai et al., 2019) and the isotopic composition of local precipitation modified by evaporation (Zaarur et al., 2011; Dong et al., 2020). Different species grow in seasons with different temperatures (Wang et al., 2016; Zhai et al., 2019), precipitation $\delta^{18}O_{water}$ values, and relative humidity. Furthermore, because individual snails are short lived, considerable variation in the temperatures and $\delta^{18}O_{water}$ values recorded by land-snail individuals is expected (Eagle et al., 2013). This variability is further exacerbated because the recorded clumped isotope temperatures depend on shell properties such as shell color and morphology, and the ecological behavior of the snail (Zaarur et al., 2011). Accordingly, the observed variability among individual snail-shell $T(\Delta_{47})$ and reconstructed $\delta^{18}O_{water}$ values within a single horizon is expected; however, this natural variability can mask and complicate interpretation of environmental shifts in the proxy records.

Land-snail shells, following embedding in loess and paleosol, might also have undergone recrystallization and associated re-equilibration of shell carbonate isotopic values due to dissolution and re-precipitation (Zamanian et al., 2016b, c). Hence, it is possible that recrystallization might have biased the recorded temperatures toward warmer, post-burial environmental conditions. However, we are unable to determine the extent of such effects. Large $T(\Delta_{47})$ uncertainties for some analyzed biogenic carbonate samples (Table 1) further limit our ability to test the hypothesis of land-snail variability rigorously. Future studies, where it is possible to sample a large number of individual shells of each species, could achieve sufficient precision (Eagle et al., 2013).

In contrast to land-snail shells, earthworms seem to not incorporate the ingested carbonates in their biospheroliths (Moine et al., 2017). Thus, the $T(\Delta_{47})$ values ($8 \pm 2°C$) of earthworm biospheroliths likely record the temperature at the soil surface during earthworm activity. Our direct biospheroliths $T(\Delta_{47})$ measurement is within the range, but on the lower side of our average warm-season soil temperature estimate based on large rhizolith clumped isotope measurements ($14 \pm 5°C$), and the warm-season soil ($13 \pm 4°C$ to $15 \pm 3°C$) temperature ranges inferred by Prud´homme et al. (2016) for the Nussloch paleosol-loess sequence. The uncertainties are large enough to permit significant variation in biospherolith-based temperature estimates, which would not be surprising given that the carbonate samples here and in the study of Prud´homme et al. (2016) homogenize a large

number of individual earthworm granules, each of which formed in a single day. Soil carbonate formation and earthworm activity were likely both restricted to the warmest periods of year in the Nussloch permafrost environment, so we do not suggest that the low resolution of these thermometry techniques masks a seasonal difference in rhizoliths and biospheroliths formation.

Implications for paleoenvironmental reconstructions from stable isotopes of carbonates in loess and paleosol deposits

Our observations of the $\delta^{13}C$, $\delta^{18}O$, and clumped isotope temperatures of carbonate types associated with the Nussloch paleosol-loess sequence suggest several broader implications for paleoenvironmental reconstructions from these and similar deposits (Table 2, Fig. 5).

First, the contribution of detrital carbonate to bulk loess and paleosol carbonate makes these materials unsuitable for paleoenvironmental reconstruction (e.g., interpreting mean annual or seasonal air temperatures), as observed in other recent $T(\Delta_{47})$ investigations of loess-paleosol sequences (Lechler et al., 2018). The contribution of geogenic detrital carbonate was made obvious by the clumped isotope apparent temperatures well in excess of plausible Earth surface conditions. However, it is possible that in the absence of clumped isotope data, the contribution of bulk geogenic carbonate may not be recognized. Geogenic carbonate contribution may be particularly difficult to recognize in deposits where pedogenic grain coatings of carbonate formed in situ also contribute significantly to the isotopic composition of the bulk carbonate samples. In such cases, it may be possible to interpret variations in carbonate $\delta^{13}C$ and $\delta^{18}O$ to document temporal variation in the seasonality of precipitation, in vegetation or in other paleoenvironmental variables, when in reality the carbonate $\delta^{13}C$ and $\delta^{18}O$ variations may document variations in the degree of pedogenic overprinting of detrital carbonate in bulk loess or paleosol deposits. Clumped isotope data would provide a simple test of the interpretation. In addition, isotopic analysis of bulk carbonate in paleosol-loess deposits can be valuable in interpreting isotopic compositions of land-snail shells, given that many of these organisms ingest this carbonate as a significant proportion of their diet.

Second, our findings contribute to a growing body of literature concerning seasonal bias in pedogenic carbonate formation, and the implications of this bias for paleoenvironmental reconstruction (e.g., Burgener et al., 2016; Kelson et al., 2020). Most previous work on this topic has focused on carbonate pendant (clast coating) and nodule formation in modern and Holocene soils (Breecker et al., 2009; Quade et al., 2011; Peters et al., 2013; Burgener et al., 2016; Gallagher and Sheldon, 2016; Ringham et al., 2016). We complement these approaches by examining isotopic values in carbonates of different types in the same temporal horizon. The variations in carbonate $\delta^{13}C$, $\delta^{18}O$ (Fig. 2), and clumped isotope temperatures (Fig. 3) are consistent with specific mechanisms

Table 2. The suitability of $\delta^{13}C$, $\delta^{18}O$, and $T(\Delta_{47})$ values of various carbonate types at Nussloch paleosol-loess sequence for local paleoenvironmental reconstructions.

Carbonate types	$\delta^{13}C_{carbonate}$	$\delta^{18}O_{carbonate}$	$T(\Delta_{47})$
Rhizoliths small (few mm in diameter and length)	$\delta^{13}C$ of local vegetation	$\delta^{18}O$ of soil water at specific evaporative conditions during warm seasons	Warmest temperature over one (or a few) vegetation periods
Rhizoliths large (1 cm or more in diameter and length)			Mean temperature of warm seasons over many vegetation periods up to a few decades
Loess dolls (few mm in size)	Probably $\delta^{13}C$ of local vegetation		Temperature of warm events
Land-snail shells	$\delta^{13}C$ of grazed plants and organic residues ($\delta^{13}C$ of ingested bulk carbonate should be considered)		Mean temperature of warm seasons over a few years. Temperature range depends on species habitat, diet, morphology/shell color, and lifespan
Earthworm biospheroliths	$\delta^{13}C$ of grazed plants and organic residues		Mean temperature of warm seasons
Bulk CaCO₃	Cannot be used for interpretation of local conditions. Necessary to measure as a reference for interpretation of $\delta^{13}C$ of biogenic & pedogenic carbonates	May include contribution from detrital source rock, pedogenic grain coatings, or other sources	Not applicable for reconstructing local conditions. Reflect the formation conditions before deposition to some degree. Clumped isotope values can be used to assess the presence or absence of detrital material

of carbonate formation that integrate environmental information over time periods, which we suggest may range from a single vegetation growth event in small rhizoliths, to decades and centuries of summers in larger rhizoliths. Together, our interpretations provide guidance for sampling strategies, to consider time resolution in future studies. Such studies may target carbonates that grow over short periods to examine seasonal variability and extremes, and carbonates that grow over longer periods to document seasonal average temperatures and representative vegetation and precipitation isotopic values (Burgener et al., 2016; Ringham et al., 2016; Ji et al., 2018; Lechler et al., 2018).

Finally, our results and those of other studies in the Nussloch remind us that pedogenic/biogenic processes as well as seasonal biases must be considered in paleoenvironmental interpretations of paleosol archives. In European paleosol-loess archives alone, reconstructions of Last Glacial paleotemperatures depend significantly on both the proxy method and the type of deposit to which the method is applied. Specific proxies may provide estimates for a particular month or average warm season air temperature (Rousseau, 1991; Moine et al., 2002), for mean annual air temperature (Renssen and Vandenberghe, 2003; Vandenberghe et al., 2014; Schatz et al., 2015), for winter air temperature (Rousseau, 1991), or for seasonally biased or mean annual soil temperature (Prud'homme et al., 2016). Mean annual temperature estimates for periods of loess formation and paleosol formation also differ from one another (Schatz et al., 2015), with paleosol formation representing milder climate conditions during interstadial events (Prud'homme et al., 2016). Better understanding of

the processes responsible for differences in proxy records as a function of the periods over which proxy materials form is needed to integrate multiple records into more complete paleoenvironmental reconstructions.

CONCLUSIONS

Various carbonate types deposited in the same paleo-horizon or layer of the Nussloch paleosol-loess sequence record specific environmental information because of differences in formation mechanisms and duration. Bulk carbonates in the Nussloch paleosol-loess sequence are detrital materials that record the diagenetic conditions of carbonates in the deflation area instead of local environmental conditions. Therefore, bulk carbonates should be excluded from samples taken to reconstruct the local paleoenvironment. We interpret small rhizoliths, loess dolls, land-snail shells, and earthworm biospheroliths as records of temperatures and soil water content that reflect environmental conditions over the short time periods over which they form. In contrast, large rhizoliths (centimeters in thickness) record mainly summer temperatures averaged over decades. This finding suggests that rhizolith size should be considered for paleoenvironmental reconstructions, with larger rhizoliths being more reliable indicators of average warm season conditions. Earthworm biospheroliths and land-snail shells are suitable materials for paleoenvironment and paleovegetation reconstructions. In the case of land snails, their ecological habit, including the proportion of ingested bulk/geogenic carbonate and the isotopic composition of bulk soil carbonates should be considered. This study highlights that with proper

consideration of proxy carbonate type and associated formation mechanisms, integrated stable (δ^{13}C, δ^{18}O) and clumped (Δ_{47}) isotopic values of pedogenic and biogenic carbonates can yield robust paleoenvironment reconstructions with decadal and even seasonal temporal resolution.

ACKNOWLEDGMENTS

SUPPLEMENTARY MATERIAL

The supplementary material for this article can be found at https://doi.org/10.1017/qua.2020.109

REFERENCES

Affek, H.P., 2012. Clumped Isotope Paleothermometry: Principles, Applications, and Challenges. *Paleontological Society Papers* 18, 101–114. https://doi.org/10.1017/S1089332600002576.

Alonso-Zarza, A.M., 1999. Initial stages of laminar calcrete formation by roots: examples from the Neogene of central Spain. *Sedimentary Geology* 126, 177–191. https://doi.org/10.1016/S0037-0738(99)00039-1.

Antoine, P., Rousseau, D.-D., Degeai, J.-P., Moine, O., Lagroix, F., Kreutzer, S., Fuchs, M., Hatte, C., Gauthier, C., Svoboda, J., Lisa, L., 2013. High-resolution record of the environmental response to climatic variations during the Last Interglacial-Glacial cycle in Central Europe: the loess-palaeosol sequence of Dolni Vestonice (Czech Republic). *Quat. Sci. Rev*. 67, 17–38. https://doi.org/10.1016/j.quascirev.2013.01.014

Antoine, P., Rousseau, D.-D., Moine, O., Kunesch, S., Hatté, C., Lang, A., Tissoux, H., Zöller, L., 2009. Rapid and cyclic aeolian deposition during the Last Glacial in European loess: a high-resolution record from Nussloch, Germany. *Quaternary Science Reviews* 28, 2955–2973. https://doi.org/10.1016/j.quascirev.2009.08.001.

Antoine, P., Rousseau, D.D., Zoller, L., Lang, A., Munaut, A.V., Hatté, C., Fontugne, M., 2001. High-resolution record of the last Interglacial-glacial cycle in the Nussloch loess-palaeosol sequences, Upper Rhine Area, Germany. *Quaternary International* 76–77, 211–229. https://doi.org/10.1016/S1040-6182(00)00104-X.

Baez-Hernandez, M., Garcia, N., Menendez, I., Jaramillo, A., Sanchez-Perez, I., Santana, A., Alonso, I., Mangas, J., Hernandez-Leon, S., 2019. Interaction of sinking behaviour of Saharan dust and lithogenic and biogenic fluxes in the Canary Basin. *Scientia Marina* 83, 121–132. https://doi.org/10.3989/scimar.04877.19A.

Balakrishnan, M., Yapp, C.J., Theler, J.L., Carter, B.J., Wyckoff, D.G., 2005. Environmental significance of ^{13}C/^{12}C and ^{18}O/^{16}O ratios of modern land-snail shells from the southern great plains of North America. *Quaternary Research* 63, 15–30. https://doi.org/10.1016/j.yqres.2004.09.009.

Bayat, O., Karimi, A., Khademi, H., 2016. Stable isotope geochemistry of pedogenic carbonates in loess-derived soils of northeastern Iran: paleoenvironmental implications and correlation across Eurasia. *Quaternary International* 429, 52–61. https://doi.org/10.1016/j.quaint.2016.01.040.

Bernasconi, S.M., Müller, I.A., Bergmann, K.D., Breitenbach, S.F.M., Fernandez, A., Hodell, D.A., Jaggi, M., Meckler, A.N., Millan, I., Ziegler, M., 2018. Reducing uncertainties in carbonate clumped isotope analysis through consistent carbonate-based standardization. *Geochemistry, Geophysics, Geosystems* 19, 2895–2914. https://doi.org/10.1029/2017GC007385.

Birkeland, 1999. *Soils and Geomorphology (3ʳᵈ Ed.)*. Oxford, Oxford University Press.

Boschi, C., Kappeler, M., Tanner, K.M., 2011. *Die Schneckenfauna der Schweiz: Ein umfassendes Bild- und Bestimmungsbuch (1st Ed.)*. Haupt Verlag, Bern.

Breecker, D.O., Sharp, Z.D., McFadden, L.D., 2009. Seasonal bias in the formation and stable isotope composition of pedogenic carbonate in modern soils from central New Mexico. *Geological Society of America Bulletin* 121, 630–640. https://doi.org/10.1130/B26413.1.

Burgener, L., Huntington, K.W., Hoke, G.D., Schauer, A., Ringham, M.C., Latorre, C., Díaz, F.P., 2016. Variations in soil carbonate formation and seasonal bias over >4 km of relief in the western Andes (30°S) revealed by clumped isotope thermometry. *Earth and Planetary Science Letters* 441, 188–199. https://doi.org/10.1016/j.epsl.2016.02.033.

Burgener, L., Hyland, E., Huntington, K.W., Kelson, J.R., Sewall, J.O., 2019. Revisiting the equable climate problem during the Late Cretaceous greenhouse using paleosol carbonate clumped isotope temperatures from the Campanian of the Western Interior Basin, USA. *Palaeogeography, Palaeoclimatology, Palaeoecology* 516, 244–267. https://doi.org/10.1016/j.palaeo.2018.12.004.

Cameron, R.A.D., 1970. The effect of temperature on the activity of three species of helicid snail (Mollusca: Gastropoda). *Journal of Zoology* 162, 303–315. https://doi.org/10.1111/j.1469-7998.1970.tb01267.x.

Canti, M.G., 2009. Experiments on the origin of C-13 in the calcium carbonate granules produced by the earthworm Lumbricus terrestris. *Soil Biol. Biochem*. 41, 2588–2592. https://doi.org/10.1016/j.soilbio.2009.09.007

Catoni, M., Falsone, G., Bonifacio, E., 2012. Assessing the origin of carbonates in a complex soil with a suite of analytical methods. *Geoderma* 175–176, 47–57. https://doi.org/10.1016/j.geoderma.2012.01.022.

Cerling, T.E., 1984. The stable isotopic composition of modern soil carbonate and its relationship to climate. *Earth and Planetary Science Letters* 71, 229–240. https://doi.org/10.1016/0012-821X(84)90089-X.

Dawson, T.E., Mambelli, S., Plamboeck, A.H., Templer, P.H., Tu, K.P., 2002. Stable isotopes in plant ecology. *Annual Review of Ecology and Systematics* 33, 507–559. https://doi.org/10.1146/annurev.ecolsys.33.020602.095451.

Dennis, K.J., Affek, H.P., Passey, B.H., Schrag, D.P., Eiler, J.M., 2011. Defining an absolute reference frame for "clumped"

isotope studies of CO_2. *Geochimica et Cosmochimica Acta* 75, 7117–7131. https://doi.org/10.1016/j.gca.2011.09.025.

Dong, J., Eiler, J., An, Z., Wu, N., Liu, W., Li, X., Kitchen, N., Lu, F., 2020. Clumped and stable isotopes of land snail shells on the Chinese Loess Plateau and their climatic implications. *Chemical Geology* 533, 119414. https://doi.org/10.1016/j.chemgeo.2019.119414.

Drever, J.I., 1982. *The Geochemistry of Natural Waters.* Prentice Hall, Englewood Cliffs, New Jersey.

Eagle, R.A., Risi, C., Mitchell, J.L., Eiler, J.M., Seibt, U., Neelin, J.D., Li, G., Tripati, A.K., 2013. High regional climate sensitivity over continental China constrained by glacial-recent changes in temperature and the hydrological cycle. *Proceedings of the National Academy of Sciences* 110, 8813–8818. https://doi.org/10.1073/pnas.1213366110.

Eiler, J.M., 2007. "Clumped-isotope" geochemistry—The study of naturally-occurring, multiply-substituted isotopologues. *Earth and Planetary Science Letters* 262, 309–327. https://doi.org/10.1016/j.epsl.2007.08.020.

Eiler, J.M., Bergquist, B., Bourg, I., Cartigny, P., Farquhar, J., Gagnon, A., Guo, W., *et al.*, 2014. Frontiers of stable isotope geoscience. *Chemical Geology* 372, 119–143. https://doi.org/10.1016/j.chemgeo.2014.02.006.

Fechter, R., Falkner, G., Steinbach, G., Wendler, F., 1990. *Weichtiere: Europäische Meeres- und Binnenmollusken.* Mosaik-Verlag, Munich.

Field, R.D., 2010. Observed and modeled controls on precipitation $\delta^{18}O$ over Europe: from local temperature to the Northern Annular Mode. *Journal of Geophysical Research D, Atmospheres* 115, D12101. https://doi.org/10.1029/2009JD013370.

Fisk, H., 1951. Loess and Quaternary geology of the Lower Mississippi Valley. *Journal of Geology* 59, 333–356. https://doi.org/10.1086/625872.

Frechen, M., Oches, E.A., Kohfeld, K.E., 2003. Loess in Europe—mass accumulation rates during the Last Glacial Period. In: Derbyshire, E. (Ed.), Loess and the Dust Indicators and Records of Terrestrial and Marine Palaeoenvironments (DIRTMAP) database. *Quaternary Science Reviews* 22, 1835–1857. https://doi.org/10.1016/S0277-3791(03)00183-5.

Gallagher, T.M., Hren, M., Sheldon, N.D., 2019. The effect of soil temperature seasonality on climate reconstructions from paleosols. *American Journal of Science* 319, 549–581. https://doi.org/10.2475/07.2019.02.

Gallagher, T.M., Sheldon, N.D., 2016. Combining soil water balance and clumped isotopes to understand the nature and timing of pedogenic carbonate formation. *Chemical Geology* 435, 79–91. https://doi.org/10.1016/j.chemgeo.2016.04.023.

Gao, Y., Li, Z., Zhu, R., Liao, H., 2020. Stable isotope compositions, sources and paleoenvironmental significance of Holocene calcareous root tubes in the Tengger Desert, Northwest China. *CATENA* 195, 104846. https://doi.org/10.1016/j.catena.2020.104846.

Garzione, C.N., Auerbach, D.J., Smith, J.J.-S., Rosario, J.J., Passey, B.H., Jordan, T.E., Eiler, J.M., 2014. Clumped isotope evidence for diachronous surface cooling of the Altiplano and pulsed surface uplift of the Central Andes. *Earth and Planetary Science Letters* 393, 173–181. https://doi.org/10.1016/j.epsl.2014.02.029.

Ghafarpour, A., Khormali, F., Balsam, W., Karimi, A., Ayoubi, S., 2016. Climatic interpretation of loess-paleosol sequences at Mobarakabad and Aghband, Northern Iran. *Quaternary Research* 86, 95–109. https://doi.org/10.1016/j.yqres.2016.05.004.

Ghosh, P., Adkins, J., Affek, H., Balta, B., Guo, W., Schauble, E.A., Schrag, D., Eiler, J.M., 2006. ^{13}C-^{18}O bonds in carbonate minerals: a new kind of paleothermometer. *Geochimica et Cosmochimica Acta* 70, 1439–1456. https://doi.org/10.1016/j.gca.2005.11.014.

Gile, L.H., Peterson, F.F., Grossman, R.B., 1966. Morphological and genetic sequences of carbonate accumulation in desert soils. *Soil Science* 101, 347–360. https://doi.org/10.1097/00010694-196605000-00001.

Gocke, M., Pustovoytov, K., Kühn, P., Wiesenberg, G.L.B., Löscher, M., Kuzyakov, Y., 2011. Carbonate rhizoliths in loess and their implications for paleoenvironmental reconstruction revealed by isotopic composition: $\delta^{13}C$, ^{14}C. *Chemical Geology* 283, 251–260. https://doi.org/10.1016/j.chemgeo.2011.01.022.

Gocke, M., Wiesenberg, G., Pustovoytov, K., Kuzyakov, Y., 2010. Rhizoliths in loess - a new tool to estimate post-sedimentary incorporation of organic matter in terrestrial environments. *Org. Geochem.* 41, 1198–1206.

Guo, Z.T., Ruddiman, W.F., Hao, Q.Z., Wu, H.B., Qiao, Y.S., Zhu, R.X., Peng, S.Z., *et al.*, 2002. Onset of Asian desertification by 22 Myr ago inferred from loess deposits in China. *Nature* 416, 159–163. https://doi.org/10.1038/416159a.

Haase, D., Fink, J., Haase, G., Ruske, R., Pécsi, M., Richter, H., Altermann, M., Jäger, K.-D., 2007. Loess in Europe—its spatial distribution based on a European Loess Map, scale 1:2,500,000. *Quaternary Science Reviews* 26, 1301–1312. https://doi.org/10.1016/j.quascirev.2007.02.003.

Hatté, C., Antoine, P., Fontugne, M., Rousseau, D.-D., Tisnérat-Laborde, N., Zöller, L., 1999. New chronology and organic matter paleoclimatic significance of Nußloch loess sequence (Rhine Valley, Germany). *Quaternary International* 62, 85–91.

Hatté, C., Fontugne, M., Rousseau, D.D., Antoine, P., Zoller, L., Tisnerat-Laborde, N., Bentaleb, I., 1998. $\partial^{13}C$ variations of loess organic matter as a record of the vegetation response to climatic changes during the Weichselian. *Geology* 26, 583–586. https://doi.org/10.1130/0091-7613(1998)026<0583:CVOLOM>2.3.CO;2.

He, B., Olack, G.A., Colman, A.S., 2012. Pressure baseline correction and high-precision CO_2 clumped-isotope (Δ_{47}) measurements in bellows and micro-volume modes. *Rapid Communications in Mass Spectrometry* 26, 2837–2853. https://doi.org/10.1002/rcm.6436.

Huguet, A., Bernard, S., Khatib, R.E., Gocke, M.I., Wiesenberg, G.L.B., Derenne, S., 2020. Multiple stages of plant root calcification deciphered by chemical and micromorphological analyses. *Geobiology.* https://doi.org/10.1111/gbi.12416.

Huntington, K.W., Eiler, J.M., Affek, H.P., Guo, W., Bonifacie, M., Yeung, L.Y., Thiagarajan, N., Passey, B., Tripati, A., Daëron, M., Came, R., 2009. Methods and limitations of 'clumped' CO_2 isotope (Δ_{47}) analysis by gas-source isotope ratio mass spectrometry. *Journal of Mass Spectrometry* 44, 1318–1329. https://doi.org/10.1002/jms.1614.

Huntington, K.W., Lechler, A.R., 2015. Carbonate clumped isotope thermometry in continental tectonics. *Tectonophysics* 647–648, 1–20. https://doi.org/10.1016/j.tecto.2015.02.019.

Huth, T.E., Cerling, T.E., Marchetti, D.W., Bowling, D.R., Ellwein, A.L., Passey, B.H., 2019. Seasonal bias in soil carbonate formation and its implications for interpreting high-resolution paleoarchives: evidence from southern Utah. *JGR Biogeosciences* 124, 616–632. https://doi.org/10.1029/2018JG004496.

Ji, S., Nie, J., Lechler, A., Huntington, K.W., Heitmann, E.O., Breecker, D.O., 2018. A symmetrical CO_2 peak and asymmetrical climate change during the middle Miocene. *Earth and Planetary Science Letters* 499, 134–144. https://doi.org/10.1016/j.epsl.2018.07.011.

Karimi, A., Frechen, M., Khademi, H., Kehl, M., Jalalian, A., 2011. Chronostratigraphy of loess deposits in northeast Iran. In:

Frechen, M. (Ed.), Loess in Eurasia. *Quaternary International* 234, 124–132. https://doi.org/10.1016/j.quaint.2009.08.002.

Kelson, J.R., Huntington, K.W., Breecker, D.O., Burgener, L.K., Gallagher, T., Hoke, G., Petersen, S.V., 2020. A proxy for all seasons? A synthesis of clumped isotope data from Holocene soil carbonates. *Quaternary Science Reviews* 234, 106259. https://doi.org/10.1016/j.quascirev.2020.106259.

Kerney, M., Cameron, R.A.D., 1979. *A Field Guide to the Land Snails of Britain and North-West Europe (1st Ed.)*. Collins, London.

Kim, S.-T., O'Neil, J.R., 1997. Equilibrium and nonequilibrium oxygen isotope effects in synthetic carbonates. *Geochimica et Cosmochimica Acta* 61, 3461–3475. https://doi.org/10.1016/S0016-7037(97)00169-5.

Klappa, C.F., 1980. Rhizoliths in terrestrial carbonates: classification, recognition, genesis and significance. *Sedimentology* 27, 613–629.

Kyuma, K., Wang, Y., Tulaphitak, T., Yue, L., Araki, S., Miao, J., 1985. Paleosols in the Luochuan Loess Section 2. Degree of weathering and estimation of paleoclimate. *Soil Science and Plant Nutrition* 31, 277–286. https://doi.org/10.1080/00380768.1985.10557433.

Lambers, H., Mougel, C., Jaillard, B., Hinsinger, P., 2009. Plant-microbe-soil interactions in the rhizosphere: an evolutionary perspective. *Plant and Soil* 321, 83–115. https://doi.org/10.1007/s11104-009-0042-x.

Lang, A., Hatté, C., Rousseau, D.D., Antoine, P., Fontugne, M., Zoller, L., Hambach, U., 2003. High-resolution chronologies for loess: comparing AMS ^{14}C and optical dating results. *Quaternary Science Reviews* 22, 953–959. https://doi.org/10.1016/S0277-3791(03)00035-0.

Lechler, A.R., Huntington, K.W., Breecker, D.O., Sweeney, M.R., Schauer, A.J., 2018. Loess-paleosol carbonate clumped isotope record of late Pleistocene–Holocene climate change in the Palouse region, Washington State, USA. *Quaternary Research* 90, 331–347. https://doi.org/10.1017/qua.2018.47.

Liu, T., Guo, Z., Wu, N., Lu, H., 1996. Prehistoric vegetation on the Loess Plateau: steppe or forest? *Journal of Southeast Asian Earth Sciences* 13, 341–346. https://doi.org/10.1016/0743-9547(96)00041-4.

Li, Z., Wang, N., Cheng, H., Ning, K., Zhao, L., Li, R., 2015. Formation and environmental significance of late Quaternary calcareous root tubes in the deserts of the Alashan Plateau, northwest China. In: Marković, S., Catto, N., O'Hara-Dhand, K., McLaren, S. (Eds.), Loess and Dust: Contributions in Honour of Ian Smalley. *Quaternary International* 372, 167–174. https://doi.org/10.1016/j.quaint.2014.11.021.

Matteucci, R., Belluomini, G., Manfra, L., 2007. Late Holocene environmental change in the coastal southern Somalia inferred from Achatina and rhizoliths. *Journal of African Earth Sciences* 49, 79–89. https://doi.org/10.1016/j.jafrearsci.2007.07.001.

Meckler, A.N., Ziegler, M., Millán, M.I., Breitenbach, S.F.M., Bernasconi, S.M., 2014. Long-term performance of the Kiel carbonate device with a new correction scheme for clumped isotope measurements. *Rapid Communications in Mass Spectrometry* 28, 1705–1715. https://doi.org/10.1002/rcm.6949.

Medeiros, J.S., Ward, J.K., 2013. Increasing atmospheric [CO_2] from glacial to future concentrations affects drought tolerance via impacts on leaves, xylem and their integrated function. *New Phytology* 199, 738–748. http://doi.org/10.1111/nph.12318.

Metref, S., Rousseau, D.D., Bentaleb, I., Labonne, M., Vianey-Liaud, M., 2003. Study of the diet effect on delta ∂^{13}C of shell carbonate of the land snail *Helix aspersa* in experimental

conditions. *Earth and Planetary Science Letters* 211, 381–393. https://doi.org/10.1016/S0012-821X(03)00224-3.

Moine, O., Antoine, P., Hatte, C., Landais, A., Mathieu, J., Prud'homme, C., Rousseau, D.-D., 2017. The impact of Last Glacial climate variability in west-European loess revealed by radiocarbon dating of fossil earthworm granules. *Proc. Natl. Acad. Sci. U. S. A.* 114, 6209–6214. https://doi.org/10.1073/pnas.1614751114

Moine, O., Rousseau, D.-D., Antoine, P., 2008. The impact of Dansgaard-Oeschger cycles on the loessic environment and malacofauna of Nussloch (Germany) during the Upper Weichselian. *Quaternary Research* 70, 91–104. https://doi.org/10.1016/j.yqres.2008.02.010.

Moine, O., Rousseau, D.-D., Jolly, D., Vianey-Liaud, M., 2002. Paleoclimatic reconstruction using mutual climatic range on terrestrial mollusks. *Quaternary Research* 57, 162–172. https://doi.org/10.1006/qres.2001.2286.

Muhs, D.R., 2007. Loess deposits, origins and properties. In: Elias, S.A. (Ed.), *Encyclopedia of Quaternary Science*. Elsevier, Oxford, pp. 1405–1418. https://doi.org/10.1016/B0-44-452747-8/00158-7.

Passey, B.H., Robinson, T.F., Ayliffe, L.K., Cerling, T.E., Sponheimer, M., Dearing, M.D., Roeder, B.L., Ehleringer, J.R., 2005. Carbon isotope fractionation between diet, breath CO2, and bioapatite in different mammals. *J. Archaeol. Sci.* 32, 1459–1470. https://doi.org/10.1016/j.jas.2005.03.015

Petersen, S.V., Defliese, W.F., Saenger, C., Daëron, M., Huntington, K.W., John, C.M., Kelson, J.R., *et al.*, 2019. Effects of Improved 17O Correction on Interlaboratory Agreement in Clumped Isotope Calibrations, Estimates of Mineral-Specific Offsets, and Temperature Dependence of Acid Digestion Fractionation. *Geochemistry, Geophysics, Geosystems* 20, 3495–3519. https://doi.org/10.1029/2018GC008127.

Peters, N.A., Huntington, K.W., Hoke, G.D., 2013. Hot or not? Impact of seasonally variable soil carbonate formation on paleotemperature and O-isotope records from clumped isotope thermometry. *Earth and Planetary Science Letters* 361, 208–218. https://doi.org/10.1016/j.epsl.2012.10.024.

Pigati, J.S., Rech, J.A., Nekola, J.C., 2010. Radiocarbon dating of small terrestrial gastropod shells in North America. *Quaternary Geochronology* 5, 519–532. https://doi.org/10.1016/j.quageo.2010.01.001.

Pokryszko, B.M., 2001. Observations on seasonal dynamics of age structure and reproduction of *Pupilla muscorum* L. (Gastropoda: Pulmonata: Pupillidae). *Folia Malacologia* 9, 45–50. https://doi.org/10.12657/folmal.009.006.

Prud'homme, C., Lécuyer, C., Antoine, P., Hatté, C., Moine, O., Fourel, F., Amiot, R., Martineau, F., Rousseau, D.-D., 2018. δ^{13}C signal of earthworm calcite granules: a new proxy for palaeoprecipitation reconstructions during the Last Glacial in western Europe. *Quaternary Science Reviews* 179, 158–166. https://doi.org/10.1016/j.quascirev.2017.11.017.

Prud'homme, C., Lécuyer, C., Antoine, P., Moine, O., Hatté, C., Fourel, F., Martineau, F., Rousseau, D.-D., 2016. Palaeotemperature reconstruction during the Last Glacial from δ^{18}O of earthworm calcite granules from Nussloch loess sequence, Germany. *Earth and Planetary Science Letters* 442, 13–20. https://doi.org/10.1016/j.epsl.2016.02.045.

Quade, J., Breecker, D.O., Daeron, M., Eiler, J., 2011. The paleoaltimetry of Tibet: an isotopic perspective. *American Journal of Science* 311, 77–115. https://doi.org/10.2475/02.2011.01.

Quade, J., Cerling, T.E., 1995. Expansion of C4 grasses in the Late Miocene of Northern Pakistan: evidence from stable isotopes in

paleosols. *Palaeogeography, Palaeoclimatology, Palaeoecology* 115, 91–116. https://doi.org/10.1016/0031-0182(94)00108-K.

Renssen, H., Vandenberghe, J., 2003. Investigation of the relationship between permafrost distribution in NW Europe and extensive winter sea-ice cover in the North Atlantic Ocean during the cold phases of the Last Glaciation. *Quaternary Science Reviews* 22, 209–223. https://doi.org/10.1016/S0277-3791(02)00190-7.

Riecken, F., 1950. Loess of Iowa with some interrelationship of soils, geology, and geography. *Geological Society of America Bulletin* 61, 1572–1573.

Ringham, M.C., Hoke, G.D., Huntington, K.W., Aranibar, J.N., 2016. Influence of vegetation type and site-to-site variability on soil carbonate clumped isotope records, Andean piedmont of Central Argentina (32–34°S). *Earth and Planetary Science Letters* 440, 1–11. https://doi.org/10.1016/j.epsl.2016.02.003.

Roberts, H.M., Muhs, D.R., Bettis, E.A., III, 2013. LOESS RECORDS | North America. In: Elias, S.A., Mock, C.J. (Eds.), *Encyclopedia of Quaternary Science (2nd Ed.)*. Elsevier, Amsterdam, pp. 620–628. https://doi.org/10.1016/B978-0-444-53643-3.00159-X.

Rodriguez-Aranda, J.P., Calvo, J.P., 1998. Trace fossils and rhizoliths as a tool for sedimentological and palaeoenvironmental analysis of ancient continental evaporite successions. *Palaeogeography, Palaeoclimatology, Palaeoecology* 140, 383–399. https://doi.org/10.1016/S0031-0182(98)00036-4.

Ross, S.M., 2003. Peirce's criterion for the elimination of suspect experimental data. *J. Eng. Technol.* 20, 38–41.

Rousseau, D.-D., 1991. Climatic transfer function from quaternary molluscs in European loess deposits. *Quaternary Research* 36, 195–209. https://doi.org/10.1016/0033-5894(91)90025-Z.

Rousseau, D.-D., Boers, N., Sima, A., Svensson, A., Bigler, M., Lagroix, F., Taylor, S., Antoine, P., 2017a. (MIS3 & 2) millennial oscillations in Greenland dust and Eurasian aeolian records —a paleosol perspective. *Quaternary Science Reviews* 169, 99–113. https://doi.org/10.1016/j.quascirev.2017.05.020.

Rousseau, D.-D., Chauvel, C., Sima, A., Hatte, C., Lagroix, F., Antoine, P., Balkanski, Y., Fuchs, M., Mellett, C., Kageyama, M., Ramstein, G., Lang, A., 2014. European glacial dust deposits: Geochemical constraints on atmospheric dust cycle modeling. *Geophys. Res. Lett.* 41, 7666–7674. https://doi.org/10.1002/2014GL061382

Rousseau, D.-D., Sima, A., Antoine, P., Hatté, C., Lang, A., Zoeller, L., 2007. Link between European and North Atlantic abrupt climate changes over the last glaciation. *Geophysical Research Letters* 34, L22713. https://doi.org/10.1029/2007GL031716.

Rousseau, D.-D., Svensson, A., Bigler, M., Sima, A., Steffensen, J.P., Boers, N., 2017b. Eurasian contribution to the last glacial dust cycle: how are loess sequences built? *Climate of the Past* 13, 1181–1197. https://doi.org/10.5194/cp-13-1181-2017.

Rousseau, D.D., Antoine, P., Hatté, C., Lang, A., Zöller, L., Fontugne, M., Othman, D.B., *et al.*, 2002. Abrupt millennial climatic changes from Nussloch (Germany) Upper Weichselian eolian records during the Last Glaciation. *Quaternary Science Reviews* 21, 1577–1582. https://doi.org/10.1016/S0277-3791(02)00034-3.

Roxy, M.S., Sumithranand, V.B., Renuka, G., 2014. Soil heat flux and day time surface energy balance closure at astronomical observatory, Thiruvananthapuram, south Kerala. *Journal of Earth System Science* 123, 741–750. https://doi.org/10.1007/s12040-014-0437-9.

Schatz, A.-K., Scholten, T., Kühn, P., 2015. Paleoclimate and weathering of the Tokaj (Hungary) loess-paleosol sequence. *Palaeogeography, Palaeoclimatology, Palaeoecology* 426, 170–182. https://doi.org/10.1016/j.palaeo.2015.03.016.

Schauer, A.J., Kelson, J., Saenger, C., Huntington, K.W., 2016. Choice of ^{17}O correction affects clumped isotope (Δ_{47}) values

of CO_2 measured with mass spectrometry. *Rapid Communications in Mass Spectrometry* 30, 2607–2616. https://doi.org/10.1002/rcm.7743.

Sheppard, S., 1986. Igneous rocks; 3, isotopic case-studies of magmatism in Africa, Eurasia and Oceanic Islands. *Reviews in Mineralogy and Geochemistry* 16, 319–371.

Sima, A., Rousseau, D.-D., Kageyama, M., Ramstein, G., Schulz, M., Balkanski, Y., Antoine, P., Dulac, F., Hatté, C., 2009. Imprint of North-Atlantic abrupt climate changes on western European loess deposits as viewed in a dust emission model. *Quaternary Science Reviews* 28, 2851–2866. https://doi.org/10.1016/j.quascirev.2009.07.016.

Sun, Q., Wang, H., Zamanian, K., 2019a. Radiocarbon age discrepancies between the carbonate cement and the root relics of rhizoliths from the Badain Jaran and the Tengeri deserts, Northwest China. *CATENA* 180, 263–270. https://doi.org/10.1016/j.catena.2019.04.011.

Sun, Q., Xue, W., Zamanian, K., Colin, C., Duchamp-Alphonse, S., Pei, W., 2019b. Formation and paleoenvironment of rhizoliths of Shiyang River Basin, Tengeri Desert, NW China. *Quaternary International* 502B, 246–257. https://doi.org/10.1016/j.quaint.2018.06.046.

Sun, Q., Zamanian, K., Huguet, A., Fa, K., Wang, H., 2020. Characterization and formation of the pristine rhizoliths around Artemisia roots in dune soils of Tengeri Desert, NW China. *CATENA* 193, 104633. https://doi.org/10.1016/j.catena.2020.104633.

Sun, Q., Zamanian, K., Li, Y., Wang, H., Colin, C., Sun, H., 2019c. Carbonate crusts of Paleolake Zhuyeze, Tengeri Desert, China: formation mechanism and paleoenvironmental implications. *Quaternary International* 532, 157–165. https://doi.org/10.1016/j.quaint.2019.11.030.

Sun, Y., Clemens, S.C., Morrill, C., Lin, X., Wang, X., An, Z., 2012. Influence of Atlantic meridional overturning circulation on the East Asian winter monsoon. *Nature Geoscience* 5, 46–49. https://doi.org/10.1038/NGEO1326.

Taheri, M., Khormali, F., Wang, X., Amini, A., Wei, H., Kehl, M., Frechen, M., Chen, F., 2016. Micromorphology of the lower Pleistocene loess in the Iranian Loess Plateau and its paleoclimatic implications. *Quaternary International* 429B, 31–40. https://doi.org/10.1016/j.quaint.2016.01.063.

Terzer, S., Wassenaar, L.I., Araguás-Araguás, L.J., Aggarwal, P.K., 2013. Global isoscapes for $\delta^{18}O$ and δ^2H in precipitation: improved prediction using regionalized climatic regression models. *Hydrology and Earth System Sciences* 17, 4713–4728. https://doi.org/10.5194/hess-17-4713-2013.

Tranquillini, W., 1982. Frost-drought and its ecological significance. In: Lange, O.L., Nobel, P.S., Osmond, C.B., Ziegler, H. (Eds.), *Physiological Plant Ecology II. Encyclopedia of Plant Physiology (new series)*. Springer, Berlin, Heidelberg, v. 12, pp. 379–400. https://doi.org/10.1007/978-3-642-68150-9_12.

Vandenberghe, J., French, H.M., Gorbunov, A., Marchenko, S., Velichko, A.A., Jin, H., Cui, Z., Zhang, T., Wan, X., 2014. The Last Permafrost Maximum (LPM) map of the Northern Hemisphere: permafrost extent and mean annual air temperatures, 25–17ka BP. *Boreas* 43, 652–666. https://doi.org/10.1111/bor.12070.

VanDeVelde, J.H., Bowen, G.J., Passey, B.H., Bowen, B.B., 2013. Climatic and diagenetic signals in the stable isotope geochemistry of dolomitic paleosols spanning the Paleocene-Eocene boundary. *Geochimica et Cosmochimica Acta* 109, 254–267. https://doi.org/10.1016/j.gca.2013.02.005.

Wang, X., Cui, L., Zhai, J., Ding, Z., 2016. Stable and clumped isotopes in shell carbonates of land snails *Cathaica* sp. and *Bradybaena* sp. in North China and implications for ecophysiological characteristics and paleoclimate studies. *Geochemistry, Geophysics, Geosystems* 17, 219–231. https://doi.org/10.1002/2015GC006182.

Wu, N., Chen, X., Rousseau, D.D., Li, F., Pei, Y., Wu, B., 2007. Climatic conditions recorded by terrestrial mollusc assemblages in the Chinese Loess Plateau during marine Oxygen Isotope Stages 12–10. *Quaternary Science Reviews* 26, 1884–1896. https://doi.org/10.1016/j.quascirev.2007.04.006.

Yanes, Y., Delgado, A., Castillo, C., Alonso, M.R., Ibáñez, M., De la Nuez, J., Kowalewski, M., 2008. Stable isotope (δ^{18}O, δ^{13}C, and δD) signatures of recent terrestrial communities from a low-latitude, oceanic setting: endemic land snails, plants, rain, and carbonate sediments from the eastern Canary Islands. *Chemical Geology* 249, 377–392. https://doi.org/10.1016/j.chemgeo.2008.01.008.

Yanes, Y., Gutiérrez-Zugasti, I., Delgado, A., 2012. Late-glacial to Holocene transition in northern Spain deduced from land-snail shelly accumulations. *Quaternary Research* 78, 373–385. https://doi.org/10.1016/j.yqres.2012.06.008.

Yung, Y.L., Lee, T., Wang, C.-H., Shieh, Y.-T., 1996. Dust: a diagnostic of the hydrologic cycle during the Last Glacial Maximum. *Science* 271, 962–963. https://doi.org/10.1126/science.271.5251.962.

Zaarur, S., Olack, G., Affek, H.P., 2011. Paleo-environmental implication of clumped isotopes in land snail shells. *Geochimica et Cosmochimica Acta* 75, 6859–6869. https://doi.org/10.1016/j.gca.2011.08.044.

Zamanian, K., Pustovoytov, K., Kuzyakov, Y., 2016a. Pedogenic carbonates: forms and formation processes. *Earth-Science Reviews* 157, 1–17. https://doi.org/10.1016/j.earscirev.2016.03.003.

Zamanian, K., Pustovoytov, K., Kuzyakov, Y., 2016b. Cation exchange retards shell carbonate recrystallization: consequences for dating and paleoenvironmental reconstructions. *CATENA* 142, 134–138. https://doi.org/10.1016/j.catena.2016.03.012.

Zamanian, K., Pustovoytov, K., Kuzyakov, Y., 2016c. Recrystallization of shell carbonate in soil: 14C labeling, modeling and relevance for dating and paleo-reconstructions. *Geoderma* 282, 87–95. https://doi.org/10.1016/j.geoderma.2016.07.013.

Zech, M., Rass, S., Buggle, B., Loescher, M., Zoeller, L., 2012. Reconstruction of the late Quaternary paleoenvironments of the Nussloch loess paleosol sequence, Germany, using n-alkane biomarkers. *Quaternary Research* 78, 226–235. https://doi.org/10.1016/j.yqres.2012.05.006.

Zhai, J., Wang, X., Qin, B., Cui, L., Zhang, S., Ding, Z., 2019. Clumped isotopes in land snail shells over China: Towards establishing a biogenic carbonate paleothermometer. *Geochimica et Cosmochimica Acta* 257, 68–79. https://doi.org/10.1016/j.gca.2019.04.028.

Zhang, N., Yamada, K., Kano, A., Matsumoto, R., Yoshida, N., 2018. Equilibrated clumped isotope signatures of land-snail shells observed from laboratory culturing experiments and its environmental implications. *Chemical Geology* 488, 189–199. https://doi.org/10.1016/j.chemgeo.2018.05.001.

Zhang, N., Yamada, K., Suzuki, N., Yoshida, N., 2014. Factors controlling shell carbon isotopic composition of land snail *Acusta despecta sieboldiana* estimated from laboratory culturing experiment. *Biogeosciences* 11, 5335–5348. https://doi.org/10.5194/bg-11-5335-2014.

Zoller, L., Stremme, H., Wagner, G., 1988. Thermo-luminescence dating of loess-paleosol sequences in the Lower Rhine, Middle Rhine and Upper Rhine area, Federal-Republic-of-Germany. *Chemical Geology* 73, 39–62.